Remote Sensing of Environment 296 (2023) 113736

Contents lists available at ScienceDirect

Remote Sensing of Environment

journal homepage: www.elsevier.com/locate/rse

Hidden becomes clear: Optical remote sensing of vegetation reveals water table dynamics in northern peatlands

Iuliia Burdun [a,*], Michel Bechtold [b], Mika Aurela [c], Gabrielle De Lannoy [b], Ankur R. Desai [d], Elyn Humphreys [e], Santtu Kareksela [f], Viacheslav Komisarenko [g,h], Maarit Liimatainen [i,j], Hannu Marttila [i], Kari Minkkinen [k], Mats B. Nilsson [l], Paavo Ojanen [j,k], Sini-Selina Salko [a], Eeva-Stiina Tuittila [m], Evelyn Uuemaa [g], Miina Rautiainen [a]

[a] *Aalto University, School of Engineering, P.O. Box 14100, FI-00076 Aalto, Finland*
[b] *KU Leuven, Heverlee, Belgium*
[c] *Finnish Meteorological Institute, Helsinki, Finland*
[d] *University of Wisconsin-Madison, Madison, USA*
[e] *Carleton University, Department of Geography & Environmental Studies, Ottawa, Canada*
[f] *Metsähallitus, Jyväskylä, Finland*
[g] *University of Tartu, Tartu, Estonia*
[h] *Ghent University, Ghent, Belgium*
[i] *University of Oulu, Oulu, Finland*
[j] *Natural Resources Institute Finland, Oulu, Finland*
[k] *University of Helsinki, Department of Forest Sciences, Helsinki, Finland*
[l] *Swedish University of Agricultural Sciences, Umeå, Sweden*
[m] *University of Eastern Finland, School of Forest Sciences, Joensuu, Finland*

ARTICLE INFO

Edited by Dr. Marie Weiss

Keywords:
Sentinel-2
Bogs
Fens
Sphagnum
Vegetation cover
Soil moisture
Wetland
SWIR

ABSTRACT

The water table and its dynamics are one of the key variables that control peatland greenhouse gas exchange. Here, we tested the applicability of the Optical TRApezoid Model (OPTRAM) to monitor the temporal fluctuations in water table over intact, restored (previously forestry-drained), and drained (under agriculture) northern peatlands in Finland, Estonia, Sweden, Canada, and the USA. More specifically, we studied the potential and limitations of OPTRAM using water table data from 2018 through 2021, across 53 northern peatland sites, i.e., covering the largest geographical extent used in OPTRAM studies so far. For this, we calculated OPTRAM based on Sentinel-2 data with the Google Earth Engine cloud platform. First, we found that the choice of vegetation index utilised in OPTRAM does not significantly affect OPTRAM performance in peatlands. Second, we revealed that the tree cover density is a major factor controlling the sensitivity of OPTRAM to water table dynamics in peatlands. Tree cover density greater than 50% led to a clear decrease in OPTRAM performance. Finally, we demonstrated that the relationship between water table and OPTRAM often disappears when WT deepens (ranging between 0 to −100 cm, depending on the site location). We identified that the water table where OPTRAM ceases to be sensitive to variations is highly site-specific. Overall, our results support the application of OPTRAM to monitor water table dynamics in intact and restored northern peatlands with low tree cover density (below 50%) when the water table varies from shallow to moderately deep. Our study makes significant steps towards the broader implementation of optical remote sensing data for monitoring peatlands subsurface moisture conditions over the northern region.

* Corresponding author.
E-mail address: iuliia.burdun@aalto.fi (I. Burdun).

https://doi.org/10.1016/j.rse.2023.113736
Received 28 November 2022; Received in revised form 23 June 2023; Accepted 22 July 2023
Available online 27 July 2023

1. Introduction

1.1. Water table in peatlands

Peatlands are wetlands with a layer of partially decomposed plant remnants (known as peat) that can be several meters thick. The accumulation of such a thick peat layer is possible due to waterlogged conditions, meaning that the water table (WT) is close to the soil surface, and the soil is permanently wet (Kwon et al., 2022). Wet anaerobic conditions prevent plant remnants from complete decomposition and, thus, make peatlands precious ecosystems in terms of long-term carbon storage (Qiu et al., 2020). Today, peatlands cover 3% of the global land area, and the majority of peatlands are located in high latitudes (Melton et al., 2022), where they store approximately 25% (473–621 GtC) of the global soil carbon stock (Loisel et al., 2021; Yu et al., 2010). Anthropogenic impact (e.g., due to land-use change and drainage) (Hirschler and Osterburg, 2022; Menberu et al., 2016) and recent warming trends in high latitudes (Rantanen et al., 2022) have led to WT drawdown in northern peatlands (Swindles et al., 2019; Zhang et al., 2022). WT drawdown and changes in WT dynamics have the potential to impact peatlands' resilience to further warming (Lees et al., 2021; Peichl et al., 2014; Strachan et al., 2016) and may contribute to transforming peatlands from a long-term carbon sink into a source through peat oxidation, leaching of dissolved organic carbon, and peat fires (Leifeld and Menichetti, 2018; Millar et al., 2023).

Given the complex carbon budget response of peatlands to warming and WT drawdown (Helbig et al., 2022; Laine et al., 2019a, 2019b; Sulman et al., 2012; Zhong et al., 2020), northern peatlands might remain a carbon sink or become a carbon source depending on future climate change scenarios (Chaudhary et al., 2020; Huang et al., 2021; Qiu et al., 2020, 2022). The high-warming scenario (RCP8.5) suggests northern peatlands will dry and become carbon sources that may exacerbate global warming by 0.21 °C (0.09–0.49 °C) by 2300 (Qiu et al., 2022). Boreal peatlands that have been drained anthropogenically are estimated to emit 0.26 Gt CO_2 equivalent, which is 5%–10% of global annual anthropogenic CO_2 emissions (Leifeld and Menichetti, 2018; Loisel and Gallego-Sala, 2022), and this amount is expected to grow by 2100 (Chaudhary et al., 2020; Leifeld et al., 2019). Peatland restoration and rewetting could avoid these CO_2 emissions and partially reverse the changes brought by drainage (Dooley et al., 2022; Kreyling et al., 2021; Wilson et al., 2022). For this reason, ongoing peatland monitoring and restoration efforts require accurate WT information (Loisel and Gallego-Sala, 2022; Menberu et al., 2016, 2018; Wilson et al., 2022).

1.2. Reflectance properties of Sphagnum mosses depict moisture conditions in peatlands

Sphagnum mosses (also known as peat mosses) dominate northern peatland ecosystems, where they largely control hydrology, carbon cycling and successional dynamics (Rice et al., 2008; Sulman et al., 2010). Unlike vascular plants, mosses lack water-conducting tissue. Thus, water held within *Sphagnum* is usually a function of water availability through precipitation, peat moisture and WT (Gong et al., 2020; Harris et al., 2006). Thirty years ago, Vogelmann and Moss (1993) were one of the first who reported that *Sphagnum* water status could be determined by its reflectance properties and assumed that it might be monitorable using optical remote sensing. This assumption was later confirmed by Bryant and Baird (2003), who obtained promising relationships between the ratio of Short-Wave InfraRed (SWIR) and *Near-InfraRed* (NIR) reflectance and near-surface volumetric moisture content for three *Sphagnum* species.

Interestingly, Bryant and Baird (2003) found that the changes in the ratio seem to be species-specific. In the later studies, both SWIR and NIR spectra were utilised in Water Band Index (WBI), floating-position Water Band Index (fWBI) and Moisture Stress Index (MSI), which were found to correlate significantly with near-surface moisture (Harris et al., 2005; Van Gaalen et al., 2007). Similar to Bryant and Baird (2003), Harris et al. (2005) and Van Gaalen et al. (2007) obtained species-specific relationships that were probably due to differences in canopy architecture and water transport capacities of *Sphagnum* species. The results from these studies were based on moss canopy reflectance data measured in laboratory conditions; nevertheless, they provide grounds for possible issues of applying remote sensing data over a peatland with diverse *Sphagnum* species to monitor moisture conditions.

Since then, many studies have utilised airborne and satellite data-based moisture indices for monitoring peat moisture and WT in heterogeneous peatlands (Banskota et al., 2017; Harris and Bryant, 2009; Kalacska et al., 2018; Meingast et al., 2014; Pablo Arroyo-Mora et al., 2017; Tucker et al., 2022). However, initial studies showed that the relationships between SWIR- and NIR-based moisture indices and peatland moisture conditions were stronger for fine spatial resolution data and weaker for coarser-resolution data. For example, the correlation coefficient between MSI and WT decreased from 0.62 (field-measured) to 0.52 (airborne, 1.5 and 2 m spatial resolutions) (Harris et al., 2006). After that, the decrease in correlation at increasing spatial scale was shown by Harris and Bryant (2009) for field and airborne data and Meingast et al. (2014) for field data at a native resolution and rescaled to Worldview (2 m), Landsat (30 m), and MODIS (500 m) spatial resolutions. They suggested two reasons for the decrease in correlation. The first problem is the presence of mixed vegetation and, as a result, mixed relationships between moisture indices and moisture conditions within one pixel (Meingast et al., 2014). This explanation agrees with the species-specific relationships found by Bryant and Baird (2003), Harris et al. (2005), and Van Gaalen et al. (2007). The second problem is a decreasing variance of the data and, correspondingly, information content with decreasing spatial resolution (Justice et al., 2007). In this way, the loss of moisture information with decreasing sampling resolution reduces the ability of the SWIR-based moisture index to detect changes in near-surface wetness (Harris et al., 2006; Harris and Bryant, 2009).

1.3. The Optical TRApezoid Model (OPTRAM) for monitoring water table dynamics

To overcome the first problem of species-specific relationships between remotely-sensed and in situ measured parameters, the Optical TRApezoid Model (OPTRAM) was proposed (Sadeghi et al., 2017). OPTRAM is a method that leverages a physical relation between soil moisture and SWIR reflectance to derive moisture information from optical remote sensing data. Unlike other moisture indices, OPTRAM utilises two signals: vegetation chlorophyll information (Harris et al., 2005; Harris and Bryant, 2009) from the Normalised Difference Vegetation Index (NDVI) and moisture information from Shortwave infrared Transformed Reflectance (STR). OPTRAM relies on two assumptions: (i) a linear relationship between soil moisture and SWIR signal (Sadeghi et al., 2015) and (ii) a linear relationship between soil and vegetation moisture (Babaeian et al., 2019). If these assumptions are met, the OPTRAM value of a pixel is calculated based on the pixel's location within the NDVI-STR space; thus, OPTRAM values for pixels with the same STR but different NDVI values would differ. This is crucial in peatlands, where *Sphagnum* mosses, compared to most vascular plants, usually have higher reflectance in red spectra and lower in NIR and SWIR spectrum (Schaepman-Strub et al., 2009).

Encouraging results of OPTRAM performance have been demonstrated over various peatlands, including ones with little or no *Sphagnum* coverage (Burdun et al., 2020a, 2020b; Räsänen et al., 2022). For example, Burdun et al. (2020b) and Räsänen et al. (2022) obtained strong relationships between OPTRAM and WT in sedge-dominated peatlands, suggesting that in addition to *Sphagnum*, vascular plants can be used to monitor WT with OPTRAM. Accordingly, Burdun et al. (2020b) introduced a "best pixel" approach for OPTRAM, which is based

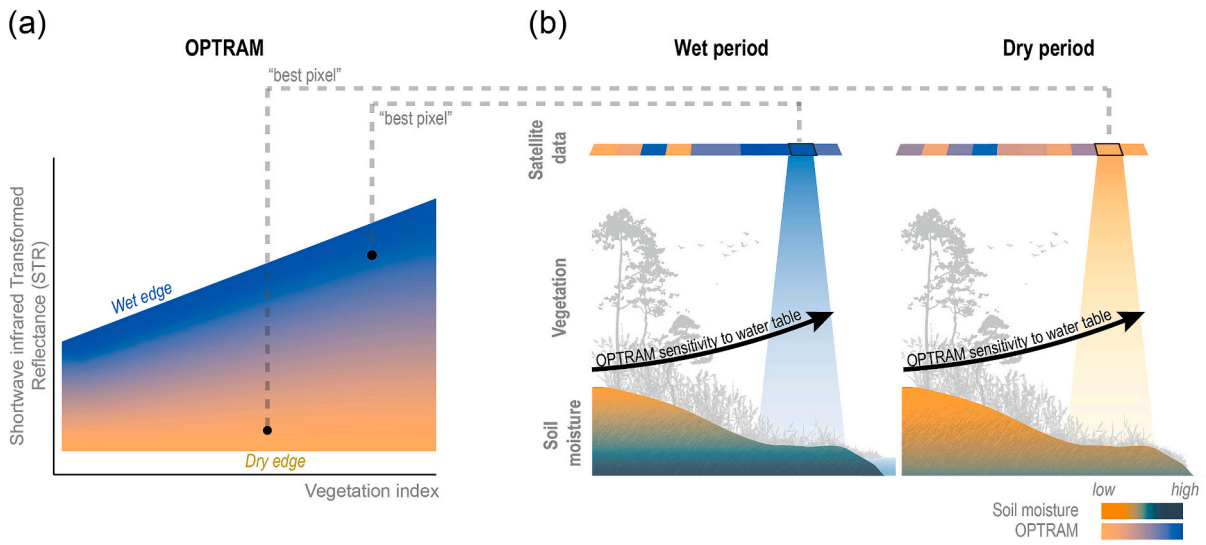

Fig. 1. Schematic illustration of the concept utilised in this work. (a) shows the STR-vegetation index (e.g., NDVI) space shaped by all the pixels of the studied peatland. In this space, dry and wet edges are defined and used for OPTRAM calculation. (b) illustrates the principle of finding one "best pixel" where OPTRAM has the highest sensitivity to temporal water table dynamics under various moisture conditions – here shown as wet and dry periods. After that, the OPTRAM time series of the "best pixel" can be used to monitor water table dynamics, assuming that water table fluctuations are synchronous in a peatland over a large area.

on finding a pixel with vegetation most sensitive to temporal changes in WT. First, such vegetation could be *Sphagnum* mosses since they do not have roots and can not control their evapotranspiration with stomata closing. Correspondingly, the water content in mosses reacts strongly to changing WT, and mosses are the first to suffer from drought stress during WT drawdown. Vascular plants also react to drought conditions, earlier than woody vegetation, through the decrease in their stomatal conductance (Laio et al., 2001).

Similar to other SWIR-based moisture indices, OPTRAM does not directly observe the position of WT; instead, it indicates vegetation moisture content (Kalacska et al., 2018). The vegetation moisture content is tightly coupled with peat moisture and WT. In peatlands, the upper peat layer has high hydraulic conductivity, which enables horizontal water movements through it (Letts et al., 2000). The high horizontal conductivity of peat leads to synchronisation in temporal changes of WT over a large area of peatland (Burdun et al., 2019; Malhotra et al., 2016; Wilson, 2012). Therefore, the WT dynamics detected in one or several "best pixels" can be extrapolated to the larger peatland area (Burdun et al., 2020b). Notice that the difference in mean values of WT and amplitude of WT fluctuations may vary across the peatland (Hokanson et al., 2018; Howie and van Meerveld, 2013).

Overall, OPTRAM (i) utilises only optical data, (ii) does not depend on the ambient atmospheric parameters and requires only one universal parametrisation for long time-series data (Babaeian et al., 2018; Sadeghi et al., 2017), and (iii) has been shown to have encouraging results over northern peatlands (Burdun et al., 2020a, 2020b; Räsänen et al., 2022). Nevertheless, OPTRAM applicability has several drawbacks and uncertainties in peatlands. First, although OPTRAM addresses the problem of species-specific relationships, it still suffers from a loss of information with decreasing spatial resolution. Burdun et al. (2020b) have demonstrated a consistent decrease in the "best pixel" correlation between OPTRAM and WT when aggregating Landsat data from 30 m to 500 m spatial resolution. Second, the effect of the tree cover density on OPTRAM sensitivity to WT has not been thoroughly investigated (Burdun et al., 2020b; Räsänen et al., 2022). Therefore, we still do not know the acceptable tree cover density for OPTRAM application in peatlands. Finally, the connection between WT and the moisture content of the uppermost peat layer could be impaired when WT is deep because of prolonged drought or disturbances such as anthropogenic drainage networks. Consequently, more research is needed to investigate the applicability of OPTRAM for WT monitoring for sites and time periods with deep WT.

1.4. Information value of spectral vegetation indices in peatlands

Vegetation information provided by NDVI is one of the key inputs to OPTRAM. NDVI is a commonly used spectral vegetation index that assumes that healthy green vegetation absorbs red and reflects NIR ranges of the solar electromagnetic spectrum (Rouse et al., 1973). However, using NDVI in peatlands has its drawbacks. First, NDVI does not characterise some *Sphagnum* species' greenness (Bubier et al., 1997) and does not capture the phenological pattern in peatland with *Sphagnum* mosses (Arroyo-Mora et al., 2018). Second, in general, NDVI saturates at high vegetation biomass and depends on soil brightness (Huete, 1988; Taddeo et al., 2019). Considering these drawbacks, the applicability of OPTRAM based on NDVI might be less accurate in peatlands dominated by mosses or with closed tree canopies or in recently restored peatlands with low vegetation coverage.

To account for the drawbacks of NDVI, other vegetation indices have been suggested. For example, Enhanced Vegetation Index (EVI) utilises the blue portion of the solar electromagnetic spectrum in addition to red and NIR to minimise both soil and atmospheric effects and overcome saturation in high-biomass conditions (Huete et al., 2002; Taddeo et al., 2019). Similar to NDVI, EVI is sensitive to gross primary production, vegetation structure and composition in peatlands (Lees et al., 2020; Taddeo et al., 2019). Another example is a refined NDVI – Red-Edge NDVI (RENDVI) that utilises red edge (RE) instead of red reflectance. In peatlands, RENDVI is sensitive to total chlorophyll and nitrogen content in vegetation (Kalacska et al., 2015) and, unlike NDVI, depicts the phenological dynamics in greening (Arroyo-Mora et al., 2018). A more recently suggested index is the kernel NDVI (kNDVI) which is a good proxy of primary production and is resistant to signal saturation (Camps-Valls et al., 2021; Forzieri et al., 2022). kNDVI has a close relationship with sun-induced chlorophyll fluorescence over the peatland-dominated regions in Asia and North America (Camps-Valls et al., 2021). Nevertheless, to date, none of these vegetation indices have been tested in OPTRAM and their potential to improve WT monitoring remains unknown.

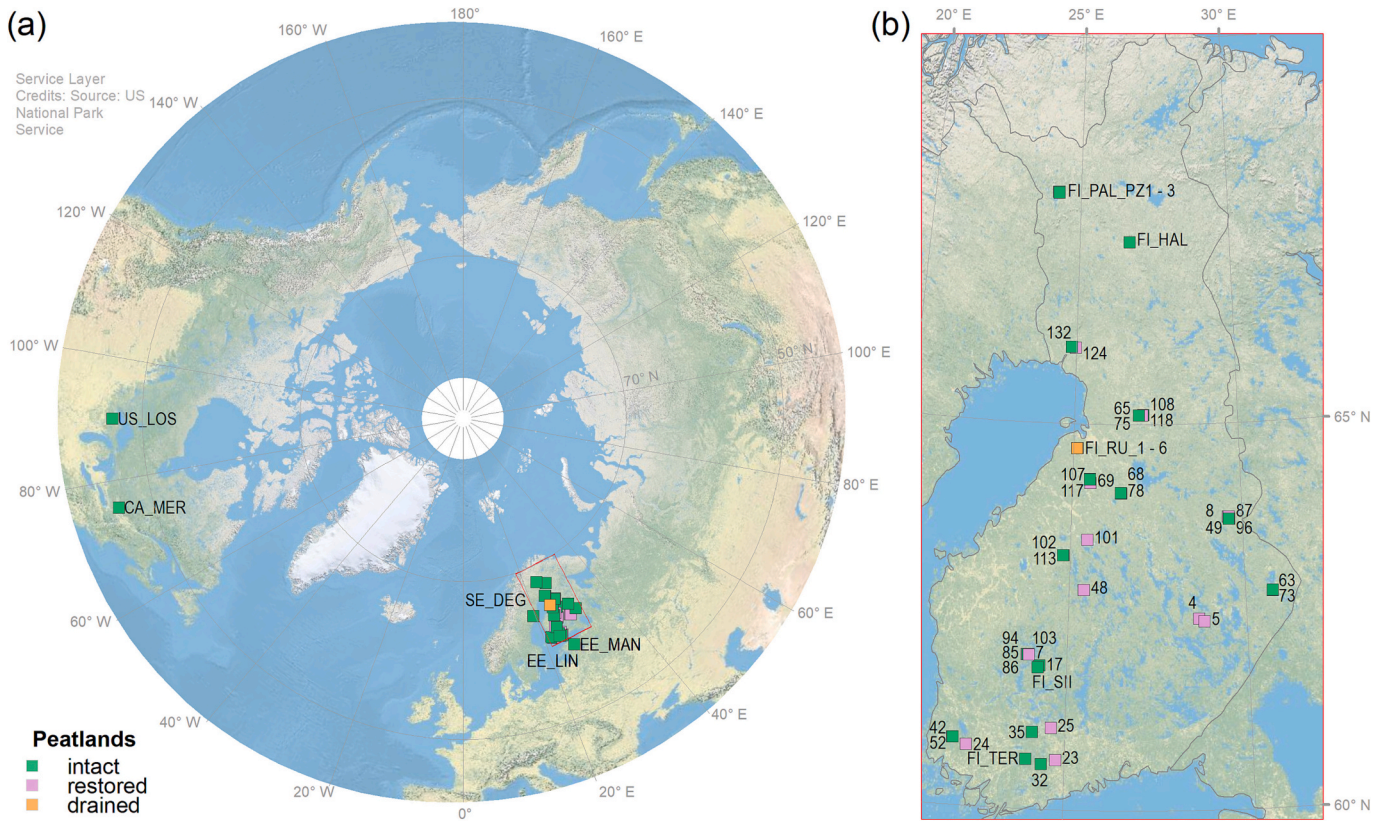

Fig. 2. Locations of the 53 peatland study areas (listed in Table S1) shown (a) for the northern hemisphere and (b) enlarged only for Finland. The colours indicate the peatlands' conditions: intact (green), restored (violet), and drained (orange). (For interpretation of the references to colour in this figure legend, the reader is referred to the web version of this article.)

1.5. Conceptual framework

Here, we hypothesise that OPTRAM can indirectly depict the temporal changes in WT through remote sensing-based observations of the vegetation moisture status in peatlands (Fig. 1). Graminoids and mosses are assumed to be the most sensitive to WT deepening (Fig. 1b). In other words, when WT is deep, this vegetation will be the first to suffer from drought stress. A change in vegetation moisture status should be detectable in the site-specific NDVI-STR space used for OPTRAM calculation (Fig. 1a). Correspondingly, the OPTRAM estimates for the pixel predominantly covered with the sensitive vegetation would have the highest temporal correlation metrics with WT over the peatland (hereinafter – "best pixel").

In this study, we evaluate OPTRAM estimates of WT over a four year period (2018–2021) using Sentinel-2 MSI satellite images for 53 intact, drained and restored northern peatlands in Finland, Estonia, Sweden, Canada, and the USA – the largest geographical extent used in OPTRAM studies so far. The first objective was to test and discuss the utility of four vegetation indices (NDVI, kNDVI, EVI, RENDVI) in OPTRAM. The second objective was to identify the impact of tree cover density on OPTRAM. The final objective was to assess the loss of relationships between WT and OPTRAM with the deepening of WT.

2. Materials and methods

2.1. Study areas

We focused on northern peatlands of various types (from eutrophic to ombrotrophic) and conditions (intact, restored, drained) (Fig. 2, Table S1). The surface areas of the studied peatlands vary greatly: from 0.04 ha (site 132) to 13.38 ha (site CA_MER). The intact sites include peatlands with little to no human disturbance. Most of the intact sites are in Finland, and a few are in Estonia, Sweden, Canada, and the USA to ensure the best geographical coverage and various conditions of peatlands.

All the studied restored peatlands are part of the Finnish network for peatland restoration monitoring. These sites were drained for forestry between the 1950s and 1970s (Räsänen et al., 2022). Restoration activities were conducted between 2007 and 2013, including an increase in WT by blocking the ditches and removing some trees to mimic the site-specific natural pre-drainage tree stand. Although the restoration occurred ten years ago, these restored sites still differ from the intact ones by their vegetation composition, soil properties and nutrient cycling. Our dataset also includes six drained peatlands currently used for agriculture in Finland. The peat thickness for these drained sites varies from 15 to 80 cm (Yli-Halla et al., 2022).

2.2. Data

2.2.1. In-situ Water Table (WT) data

WT data measured with automatic loggers from several datasets were used in this study (Table S1). First, the data from sites named with numbers in Table S1 were provided by Parks & Wildlife Finland (Metsähallitus). Second, the Estonian Environment Agency (ILM) provided the WT data measured at daily resolution in Linnusaare (EE_LIN) and Männikjärve (EE_MAN) peatlands. Finally, data from Mer Bleue (CA_MER), Halssiaapa (FI_HA), Pallas area (FI_PAL_PZ1 – FI_PAL_PZ3) with Lompolojänkkä (FI_PAL_PZ1), Ruukki (FI_RU_1 – FI_RU_6), Siikaneva (FI_SII), Tervalamminsuo (FI_TER), Degerö Stormyr (SE_DEG), and Lost Creek (US_LOS) peatlands were measured at hourly and daily temporal resolutions. To align the in situ WT data acquisition with remotely sensed data for the sites where WT was measured at hourly

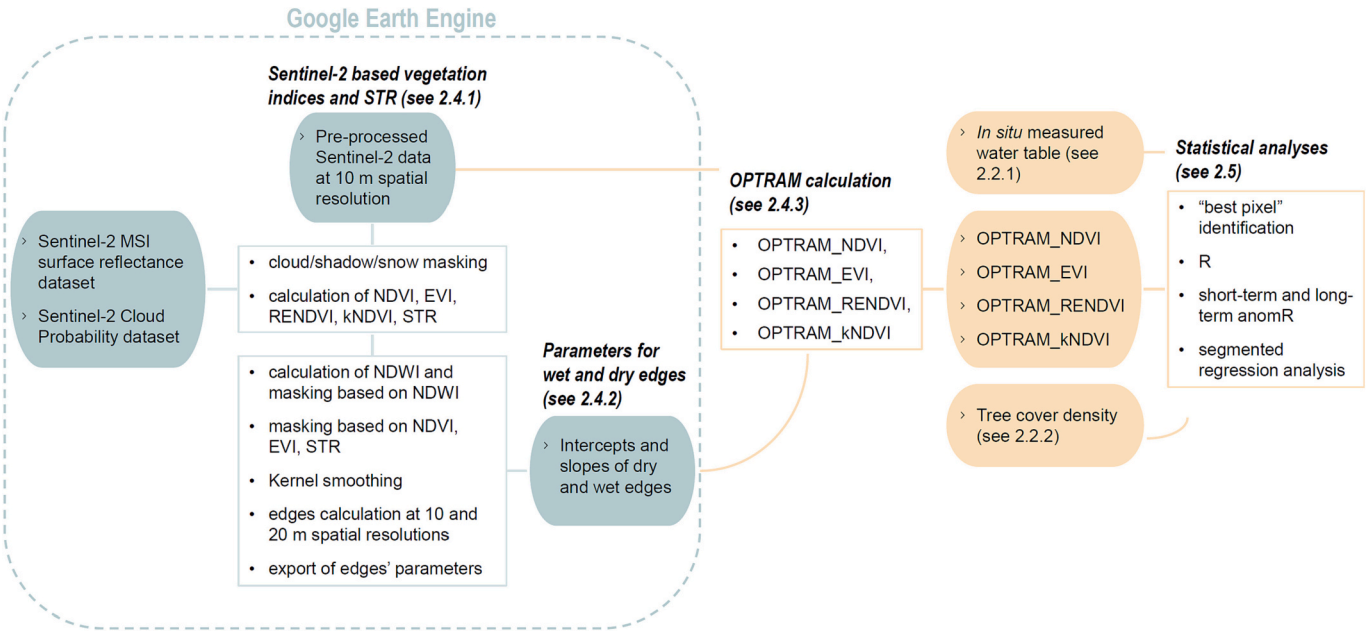

Fig. 3. General workflow of data processing in this study.

Table 1
Equations for the spectral vegetation indices and SWIR transformed reflectance used in this study based on Sentinel-2 data. The spectral band names refer to atmospherically corrected reflectance factors in given wavelengths (central wavelengths for the spectral bands are: B2: 490 nm, B4: 665 nm, B5: 705 nm, B6: 740 nm; B8: 842 nm, B12: 2190 nm).

Name	Abbreviation	Equation (Sentinel-2 reflectance bands)	Reference
Normalised difference vegetation index	NDVI	$\frac{NIR_{B8} - Red_{B4}}{NIR_{B8} + Red_{B4}}$	(Rouse et al., 1973)
Enhanced vegetation index	EVI	$\frac{2.5 \times (NIR_{B8} - Red_{B4})}{NIR_{B8} + 6 \times Red_{B4} - 7.5 \times Blue_{B2} + 1}$	(Huete et al., 2002)
Red-edge normalised difference vegetation index	RENDVI	$\frac{NIR_{B6} - NIR_{B5}}{NIR_{B6} + NIR_{B5}}$	(Arroyo-Mora et al., 2018; Gitelson and Merzlyak, 1994)
Kernel normalised difference vegetation index	kNDVI	$tanh(NDVI^2)$	(Camps-Valls et al., 2021)
Shortwave infrared transformed reflectance	STR	$\frac{(1 - SWIR_{B12})^2}{2 \times SWIR_{B12}}$	(Sadeghi et al., 2015)

temporal resolution, we averaged data to daily (midnight to midnight, local time) mean WT values.

2.2.2. Tree cover density

To estimate the impact of tree cover on OPTRAM performance in peatlands, we used the Tree Cover Density dataset for 2018 (European Environment Agency, 2018). This dataset has a high spatial resolution of 10 m and overall thematic accuracy of 85–90%. The Tree Cover Density dataset provides information on the proportional crown coverage per pixel from 0% to 100%. Since this dataset has European coverage, we estimated the tree cover impact on OPTRAM only over the peatlands located in Estonia, Sweden, and Finland, except for peatlands FI_RU_1 – FI_RU_6 since agriculture fields assigned as non-tree covered areas in the Tree Cover Density dataset.

2.2.3. Sentinel-2 satellite imagery

We used the Copernicus Sentinel-2 MSI Level-2A surface reflectance dataset (European Space Agency, 2015) that is orthorectified and atmospherically corrected and available in a cloud-based platform Google Earth Engine (GEE) (Gorelick et al., 2017). The data were taken from April to September 2018–2021. Additionally, we utilised the Sentinel-2 Cloud Probability dataset to mask clouds, shadows and snow that is available in GEE.

2.3. Data processing

The data processing workflow is shown in Fig. 3. Shortly, Sentinel-2 images were processed in GEE. First, we clipped satellite data to the studied peatland polygons and exported vegetation indices and STR (see 2.4.1); second, we exported parameters needed for calculating the dry and wet edges of OPTRAM (see 2.4.2). The final OPTRAM calculation was done in R software (R Core Team, 2022) (see 2.4.3, 2.5).

2.3.1. Processing of Sentinel-2-based vegetation indices and STR

We calculated four vegetation indices (Table 1) and STR for each Sentinel-2 image within the peatlands' polygons. Next, we exported the data from GEE at 10 m spatial resolutions.

2.3.2. Calculation of parameters for wet and dry edges

OPTRAM performance is known to suffer from oversaturated pixels, e.g., pixels covered by standing water or wet vegetation (Babaeian et al., 2018; Sadeghi et al., 2017). Oversaturated pixels have high STR values and influence the wrong estimation of wet edge (Sadeghi et al., 2017). To exclude the oversaturated pixels from our analyses, we constructed a water mask based on Normalised Difference Water Index (NDWI), calculated as follows:

$$NDWI = \frac{Green_{B3} - NIR_{B8}}{Green_{B3} + NIR_{B8}},$$

where $Green_{B3}$ and NIR_{B8} correspond to bands 3 and 8 in the Sentinel-2 MSI dataset (Gao, 1996). Visually, we identified that NDWI values greater than −0.2 corresponded to shallow ponds, temporarily flooded hollows, and ponds with floating mats of mosses in the studied peatlands. Correspondingly, NDWI values greater than −0.2 were masked from further analyses.

NDVI–STR space used for OPTRAM calculation is constrained by two isopleths of uniform soil moisture conditions in different vegetation covers: so-called wet and dry edges (Fig. 1) (Carlson, 2007). The wet edge is formed by the pixels with the highest STR values along the NDVI gradient, and these pixels are assumed to have the wettest conditions. The other way round, the dry edge is formed by the pixels with the lowest STR values along the NDVI gradient with the lowest moisture availability. NDVI–STR space is constructed using a time series of all pixels within the studied site. In previous studies, wet and dry edges were identified visually; while in our study, we aimed to optimise this process with automatic edge estimation in GEE due to the large number of studied sites. However, with the developed algorithm, we could not reliably detect the wet and dry edges for sites with less than 25,000 total pixels. Therefore, we excluded from our analysis sites with fewer than 25,000 pixels resulting from small peatland areas or frequent cloud coverage. In this way, we used data only from 36 (listed in Table S1) out of 50 peatlands initially provided by Metsähallitus. For the sites with more than 25,000 pixels, we calculated four vegetation indices presented in Table 1.

Although we applied the cloud and shadow masking, the visual analysis still identified some pixels of poor quality that affected the STR signal and could potentially lead to the miscalculation of the wet edge. Thus, first, we used additional masking and kept the pixels which were not predominantly covered by water and correspondingly, their NDVI values varied from 0 to 1 (Defries and Townshend, 2007). Second, we filtered out pixels with erroneous EVI values (values outside the range −1–1) since they could be due to cloud impact (White et al., 2019). Third, we filtered out high STR values since they could indicate oversaturated pixels. Since in previous works, the locations of wet edge were identified within the STR range approximately between 0 and 15 (Ambrosone et al., 2020; Babaeian et al., 2018; Chen et al., 2020; Mokhtari et al., 2023), we utilised STR values below 20. After that, we applied a Kernel smooth function with a 10 m radius to vegetation indices and STR in order to minimise the impact of poor quality or oversaturated pixels that could remain in the data.

Next, we proceeded to the site-specific calculation of wet and dry edges in GEE. As it was shown previously by Babaeian et al. (2018), the dry edge estimation might suffer from the missing dry pixels with high NDVI values. Thus, we limited the range of each vegetation index, within which maximal (wet edge) and minimal (dry edge) STR values would be derived. Similarly to (Ambrosone et al., 2020; Babaeian et al., 2018), we identified these ranges visually by examining NDVI–STR spaces for the studied sites. Finally, edges were calculated within the following ranges: from 0.1 to 0.7 for NDVI, from 0 to 0.6 for EVI and kNDVI, and from 0 to 0.4 for RENDVI (Fig. S1).

Our algorithm for identifying the edges is similar to the one in (Sadeghi et al., 2017) and is presented in Appendix A. For most sites, the site-specific edges were calculated for the data at an initial 10 m spatial resolution (Fig. S1). However, for the sites with a big area and high temporal data frequency, we could not estimate edges' parameters at 10 m spatial resolution due to the computational limits of GEE. Therefore, for seven sites (FI_TER, FI_SII, FI_HAL, EE_LIN, CA_MER, SE_DEG and US_LOS), the edges were calculated at a rescaled 20 m spatial resolution. We did not perform our analysis at 20 m spatial resolution for all the sites because it would lead to losing the number of pixels from comparatively small, restored sites. As a result, we would have had fewer peatlands for the analyses.

2.3.3. OPTRAM calculation

After we exported the Sentinel-2 based vegetation indices, STR, and edges parameters (slope and intercept) from GEE, we proceeded to OPTRAM calculations (Fig. 3). Based on the vegetation indices presented in Table 1, we calculated four types of OPTRAM (Fig. S2). OPTRAM for pixel i was calculated using the following equation (Sadeghi et al., 2017):

$$OPTRAM_i = \frac{STR_i - STR_{min,i}}{STR_{max,i} - STR_{min,i}},$$

where STR_i is an STR value of i pixel, $STR_{min,i}$ and $STR_{max,i}$ are the STR values of the dry and wet edges at the vegetation index value of pixel i, which can be calculated as follows (Babaeian et al., 2018):

$$STR_{min,i} = int_{min} + s_{min} \times \text{vegetation index},$$

$$STR_{max,i} = int_{max} + s_{max} \times \text{vegetation index},$$

where int_{min} and s_{min} are the intercept and slope of the dry edge, and int_{max} and s_{max} are the intercept and slope of the wet edge derived in 2.4.2.

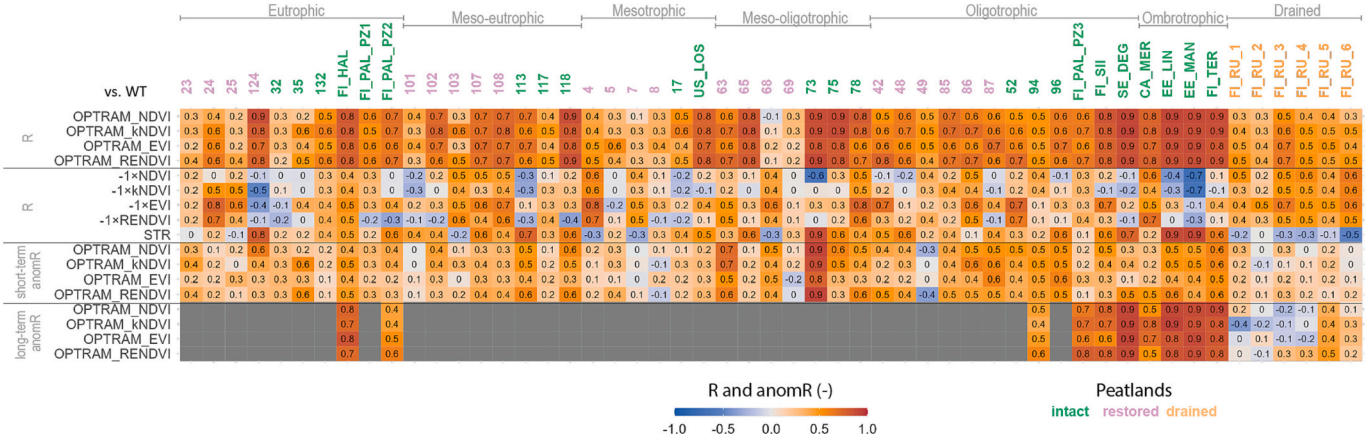

Fig. 4. Matrix with Pearson correlation coefficients (R) and two types of anomaly correlation coefficients (anomR) between in situ measured water table (WT) and OPTRAM estimates, vegetation indices multiplied by −1 for easier visual comparison, and short-wave infrared transformed reflectance (STR) at "best pixels" for all study sites. R for NDVI and STR were calculated for the "best pixels" identified with OPTRAM_NDVI. Similarly, correlation values for kNDVI, EVI and RENDVI are shown for the "best pixels" identified with OPTRAM_kNDVI, OPTRAM_EVI, and OPTRAM_RENDVI, correspondingly. Long-term anomR was calculated for the peatlands with data from at least three vegetation periods.

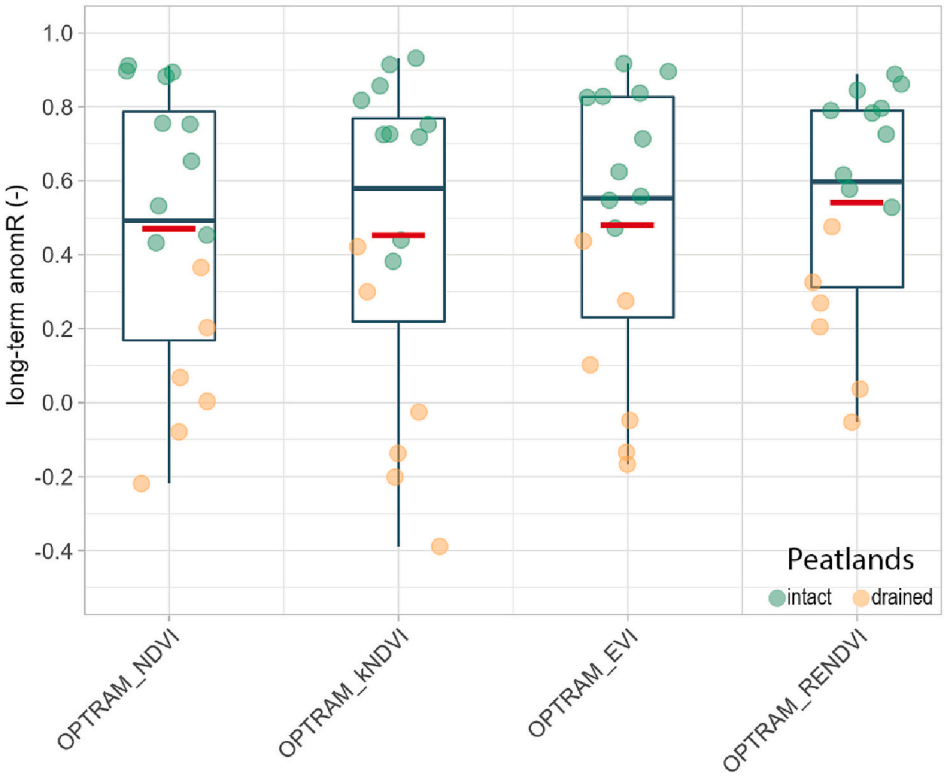

Fig. 5. Long-term anomaly correlation (long-term anomR) between OPTRAM and WT based on NDVI (OPTRAM_NDVI), kNDVI (OPTRAM_kNDVI), EVI (OPTRAM_EVI) and RENDVI (OPTRAM_RENDVI). Colours indicate peatland types, and red lines are mean values of grouped long-term anomR. (For interpretation of the references to colour in this figure legend, the reader is referred to the web version of this article.)

2.4. Statistical analyses

To test the utility of the three vegetation indices (kNDVI, EVI, RENDVI) instead of NDVI in OPTRAM, we performed Pearson correlation analysis (R), short-term Pearson anomalies correlation analysis (short-term anomR), long-term Pearson anomalies correlation analysis (long-term anomR), and *t*-test.

First, we calculated the correlation between WT and four OPTRAM estimates: OPTRAM based on NDVI (OPTRAM_NDVI), OPTRAM based on EVI (OPTRAM_EVI), OPTRAM based on RENDVI (OPTRAM_RENDVI), and OPTRAM based on kNDVI (OPTRAM_kNDVI). Later, we identified the "best pixel" as the one with the highest R-value in each studied peatland. Second, we calculated short-term and long-term anomR between WT and four OPTRAM estimates. Short-term anomR was calculated for all the peatlands as the difference between the data and the seasonality. Long-term anomR was calculated as the difference between seasonality and climatology only for the sites with at least 18 months (i.e., three years of vegetation periods) of WT data. The seasonality was derived by running a five-week moving-average window over the data in each year. The climatology was obtained as an average of the seasonality across all study years. The computation of anomR at two different timescales enables us to reveal short-term and long-term interactions between WT and OPTRAM estimates. While the short-term anomR is a skill metric to assess the ability of OPTRAM to monitor, e.g., the moisture response to rain events, the long-term anomR is a skill metric to assess the ability of OPTRAM to monitor the inter-annual variability of moisture conditions. Third, we performed the *t*-test to determine a significant difference between the mean values of anomR of OPTRAM_NDVI and other OPTRAM estimates. We also used a Shapiro-Wilk test to test the normality of data distribution and an *F-test to test the homogeneity in variances (p-value 0.05)*.

We performed a segmented regression analysis with one breaking point to reveal *the potential weakening of relationships between WT and OPTRAM*. The breaking point is here assumed to represent WT application limit of OPTRAM. *This analysis was done for the sites with deep WT (deeper than − 40 cm)*. The presence of the breaking point was tested with the *Davies test (p-value 0.05)*. *Further, we analysed only the sites with at least 10 points for each segment of the regression.*

3. Results

3.1. Performance of OPTRAM estimates based on different vegetation indices

On average, all four types of OPTRAM estimates correlated better with in situ WT than any of the STR or vegetation indices taken separately (Fig. 4). For almost all peatlands, we observed a positive correlation between WT and the "best pixel" OPTRAM estimates. STR and vegetation indices multiplied by −1 also usually positively correlated with WT.

The correlations between WT and the four vegetation indices noticeably differed for the majority of the sites (Fig. 4). Depending on the vegetation index, correlation with WT varied from positive to negative, and for some sites, e.g., FI_SII, this variation reached modulus 0.8: correlation between WT and $-1 \times$ kNDVI was −0.1, meanwhile correlation between WT and $-1 \times$ EVI was 0.7. Surprisingly, the correlation between WT and four OPTRAM estimates was less variable. For the same FI_SII peatland, both correlations between WT and OPTRAM_kNDVI, and WT and OPTRAM_EVI were 0.8.

Another interesting finding was a systematically poor performance of OPTRAM estimates in drained sites. We observed consistently low short-term anomaly correlation (Fig. 4) and the lowest long-term anomaly correlation (Fig. 4) for the drained sites. Meanwhile, ombrotrophic and oligotrophic peatlands had moderate to strong correlations, even restored sites. Short-term anomaly correlation varied from weak to strong for intact and restored peatlands. In contrast, long-term anomaly

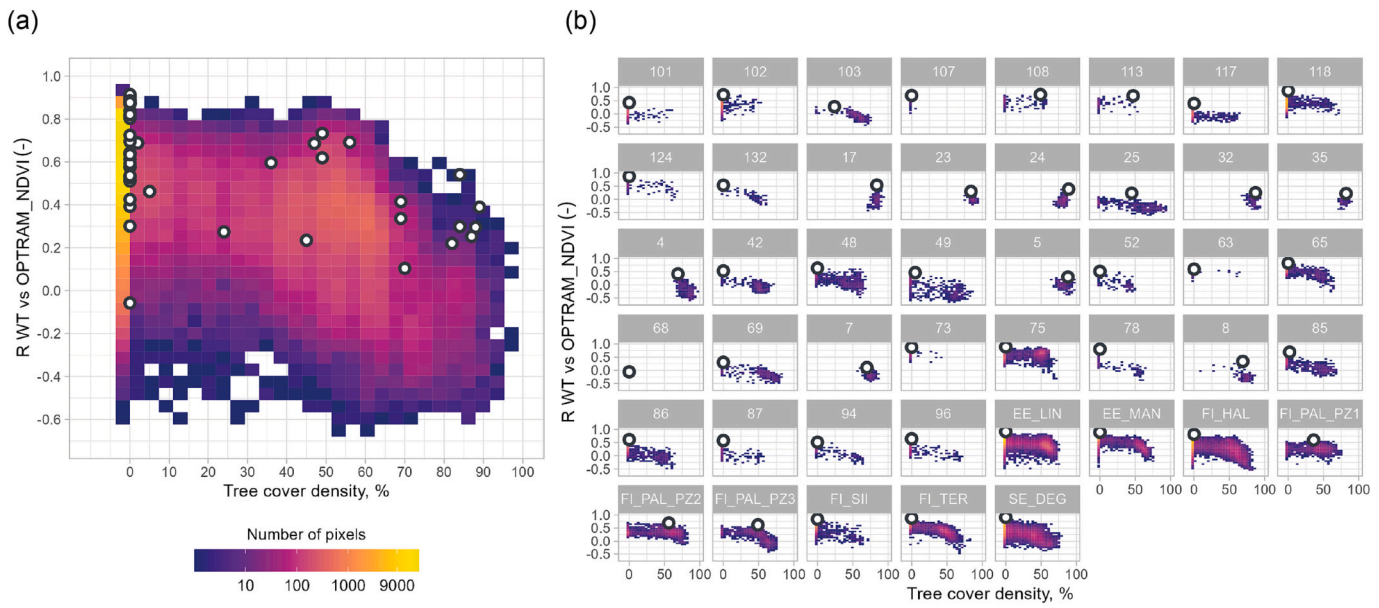

Fig. 6. Density plot between tree cover density and correlation values (R) between water table (WT) and OPTRAM based on NDVI (OPTRAM_NDVI). Points indicate the correlation and tree cover density of the "best pixels": (a) all sites shown together, and (b) separately. Note the decrease in correlation values after approximately 50% tree cover density.

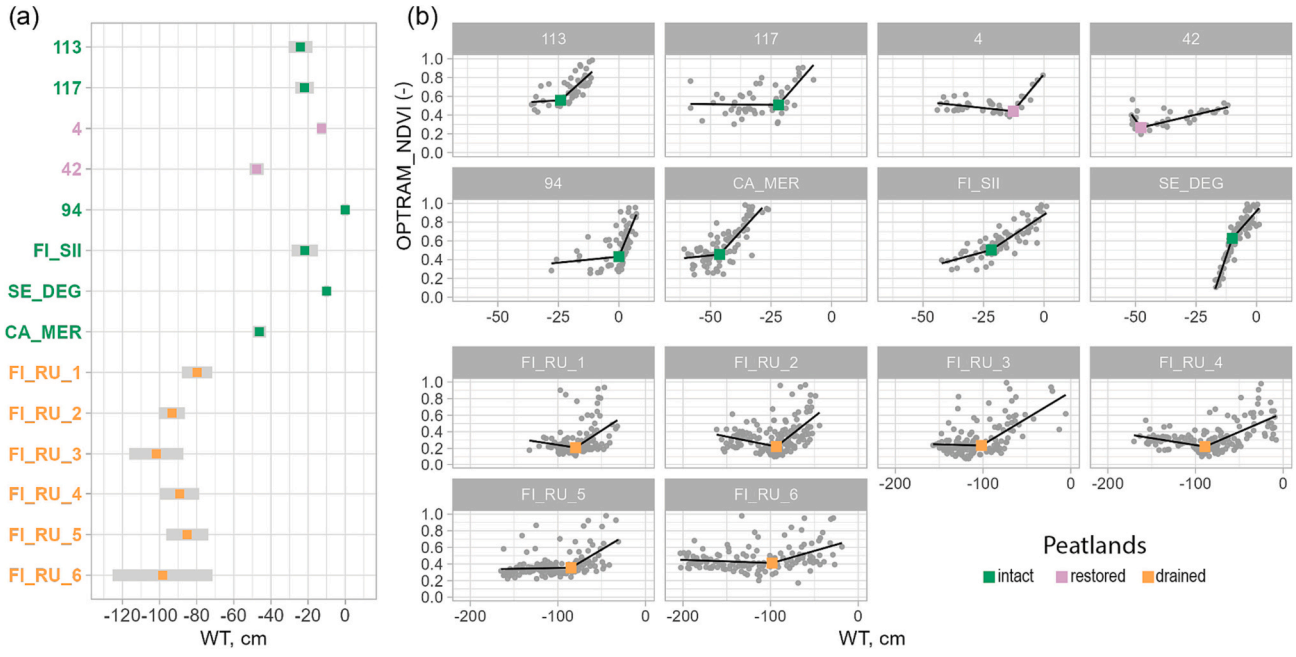

Fig. 7. Results of the segmented regression analysis. Only sites with a water table (WT) deeper than −40 cm and statistically significant (p-value <0.05) breaking points are shown. (a) shows the WT position of the breaking points with a 95% confidence interval (shaded area). (b) show the scatterplots between WT and OPTRAM_NDVI (grey point), breaking points (squared marks), and fitted linear regression (black line).

correlation values were noticeably higher than the short-term anomaly correlation values in intact peatlands (Fig. 4).

Because a t-test did not reveal significantly different mean anomaly correlation values for OPTRAM_NDVI compared with the other three OPTRAM estimates (Fig. 5), we show only the results obtained for OPTRAM_NDVI in the following.

3.2. Impact of tree cover density on OPTRAM performance

Open sites had the best performance of OPTRAM, i.e., most "best pixels" had tree cover density close to 0% (Fig. 6). The noticeable decrease in correlation between WT and OPTRAM_NDVI after the tree cover density exceeded 50% was striking.

3.3. Change in the relationships between WT and OPTRAM

The segmented regression analysis revealed that OPTRAM loses its ability to trace WT fluctuations when WT decreases below a site-specific threshold. The breaking point was identified at both deep (site 42, CA_MER) and shallow WT (site 94, SE_DEG) (Fig. 7). The deepest WT of the breaking point (below −80 cm) was observed for the drained site (FI_RU_1– FI_RU_6). As expected, for all the sites (except SE_DEG), the relationships between WT and OPTRAM_NDVI got weaker with depth.

4. Discussion

4.1. Does the choice of vegetation index affect the performance of OPTRAM?

Our findings suggest that in contrast to vegetation indices, OPTRAM is unaffected by vegetation properties and detects WT changes over heterogeneous vegetation cover. We observed that four OPTRAM estimates based on NDVI, kNDVI, EVI, and RENDVI performed similarly in the correlation and anomalies correlation analyses. The observed similarities in OPTRAM performance were surprising since we observed a noticeable variation in the correlation between WT and individual vegetation indices (Fig. 4). To illustrate this, we will use NDVI as an example. NDVI multiplied by −1 had a negative association with WT in EE_MAN (R = -0.7) and a positive association in CA_MER (R = 0.6). Nonetheless, OPTRAM performance for these sites was very similar: correlation between WT and OPTRAM_NDVI were 0.9 for EE_MAN and 0.8 for CA_MER. This result can be explained by high NDVI sensitivity to vegetation structure and composition (Taddeo et al., 2019); thus, the association of NDVI with WT has been previously reported positive (Šimanauskienė et al., 2019), negative (D'Acunha et al., 2018) or missing (Meingast et al., 2014) depending on the study site.

4.2. Why did OPTRAM fail to detect WT in some cases?

4.2.1. High tree cover density

Prior studies noticed weak sensitivity of OPTRAM to WT changes over the treed areas in peatlands (Burdun et al., 2020a, 2020b; Räsänen et al., 2022). In this study, we have shown this sensitivity of OPTRAM performance for a range of tree cover densities (Fig. 6). Particularly, a strong decrease of performance was noticeable after approximately 50% of tree cover density. We noticed this decrease in performance for peatlands covered by pines, birches, and spruces (Table S1). Unlike sedges, trees experience less water stress under the same moisture conditions (Van den Hoof and Lambert, 2016) because trees have a better adaptation to water stress due to the constitutive root system architecture (Farooq et al., 2009) and – in the case of pine and spruce – needles that are a desirable trait for drought tolerance (Farooq et al., 2009). For example, trees experience a smaller decrease in net primary production under the decreased soil moisture than grasses (Van den Hoof and Lambert, 2016). As a result, non-forested ecosystems have a higher response in greenness to changes in soil moisture than forested ecosystems (Walther et al., 2019). In line with these findings, our study shows a reduced sensitivity of OPTRAM, which is related to the vegetation moisture status, to soil moisture changes over high tree cover.

The finding of a weaker performance of OPTRAM over the treed peatlands was based on the European peatlands due to the available tree cover density dataset at high spatial resolution. Further research could be done to test our finding in other northern regions using other high spatial resolution tree cover density products (Hadi et al., 2016) and other tree species composition in peatlands.

Because the correlation between WT and OPTRAM decreased after tree cover density exceeded 50%, the applicability of OPTRAM is limited only to peatlands with sparse or no tree coverage. Moreover, these treeless or sparsely treed areas should be detectable with remote sensing data. Since peatlands have steep environmental gradients, they produce narrow ecotones that could be smaller than the spatial resolution of remote sensing data (Gallant, 2015). Therefore, utilising data with a high spatial resolution (e.g., Sentinel-2 and Landsat) should be preferable for further monitoring WT dynamics with OPTRAM.

4.2.2. Vegetation moisture content loses connection with WT when WT becomes deep

The correlation values between WT and OPTRAM varied considerably for the "best pixels" with 0% tree cover density (Fig. 7). It means that besides tree coverage, there were other factors that led to the poor performance of OPTRAM. One of these factors could be a weak relationship between vegetation moisture content and WT when WT becomes deeper. For example, the changes in WT can impact the mosses' reflectance even more than the minimal seasonal changes in pigment content (Kalacska et al., 2015). Here, we have shown that at some point of WT becoming deeper and vegetation drying, the connection between vegetation moisture content and WT disappears. We found this loss of connection at various WT (approximately from 0 to −100 cm) in 14 peatlands, including six intact, two restored and six drained sites.

The variability in critical WT at which the capillary connection gets lost can be explained by differences in peat hydraulic properties. Depending on peatland type and disturbance history, peat soils can show very different properties. Typically, degradation leads to higher bulk density, a lower macropore fraction, and much reduced hydraulic conductivity (Liu et al., 2020). The rate at which water from the saturated peat layer refills, via capillary rise, the evaporative water losses in the unsaturated peat layer depends on the peat hydraulic conductivity. A restricted capillary rise makes it more difficult for mosses and other plants to access deep water, eventually leading to an earlier loss of the connection between vegetation moisture content and WT (Potvin et al., 2015). Accordingly, heavily modified peat, in addition to the deep WT, led to poor connection between OPTRAM estimates and WT in drained sites used for agriculture (Fig. 4). Considering this, OPTRAM over drained peatlands might only be suitable for monitoring soil moisture but not WT (Babaeian et al., 2018; Sadeghi et al., 2017).

One of the studied sites was CA_MER, an ombrotrophic intact peatland with a breaking point at approximately −50 cm WT. Interestingly, for the same site, Kalacska et al. (2018) previously observed a loss in the relationship between WT and SWIR-based NDWI over the summer with the deepest WT position (also approximately −50 cm WT). Kalacska et al. (2018) explained that this relationship was lost due to the change in vegetation reflectance anisotropy and the higher impact of vascular plants on anisotropy in summer. Unfortunately, we did not find studies reporting whether the anisotropy change could lead to such significant disturbances in NDWI in peatlands. Nevertheless, a study on lingonberry and blueberry spectra suggests that the anisotropy change during the growing season is more noticeable in NIR spectra and less in SWIR (Forsström et al., 2019). Therefore, we might assume that the observed loss of sensitivity to WT of OPTRAM (in this study) and NDWI (Kalacska et al., 2018) could be due to the inability of vegetation moisture status to reflect WT changes when WT is deeper. Under this condition, the SWIR signal utilised in OPTRAM and NDWI no longer reflects WT dynamics.

This finding suggests that the applicability of OPTRAM might be limited only to the periods when WT varies from shallow to moderately deep. It also suggests utilising OPTRAM jointly with other methods that are preferable for deep WT. For example, Sentinel-1 radar backscatter data were recommended to be applied over peatlands with WT from −20 to −80 cm (Asmuß et al., 2019). The first attempt to jointly use OPTRAM and backscatter was recently made by Räsänen et al. (2022). Though, the combination of OPTRAM and backscatter data for the periods with different WT has not yet been tested.

WT deepening and afterwards increasing can also lead to another issue in monitoring WT with OPTRAM. Harris et al. (2005) revealed that water is likely to be retained in vegetation during rainfall. As a result, the vegetation moisture content would be higher after rain than after drying at the same WT (Harris and Bryant, 2009). In our study, we did not

account for this potential effect; however, in the future, the OPTRAM estimates for the days right after the rain could be treated more carefully or excluded as in studies with radar backscatter data (Bechtold et al., 2018).

The loss of the connection between WT and OPTRAM was found to occur at various WT recorded at the monitoring wells (approximately from 0 to −100 cm). However, the locations of the OPTRAMs' "best pixels" and monitoring wells did not match spatially. In other words, the WT of the detected breaking point (Fig. 7) does not correspond to the actual WT within the "best pixel". Instead, we assume that the dynamics of WT in "best pixels" and wells are synchronised. Correspondingly, we can only talk about the relative decrease or increase in WT rather than giving an absolute value of WT at the "best pixels". Thus, with the "best pixel" approach, we could not report the WT detection limits for OPTRAM. Future studies could address this knowledge gap and identify WT detection limits under controlled conditions as in (Toca et al., 2022).

4.2.3. Small variation in shallow WT

The results of this study suggest that a small variation in shallow WT could also cause a weak correlation between OPTRAM and WT. Under wet conditions, the vegetation moisture content may not reflect changes in WT in the SWIR spectrum (Wang et al., 2008). The inability of OPTRAM to monitor stable and shallow WT in peatlands was previously shown by Burdun et al. (2020b). They obtained the weakest correlation between OPTRAM and WT for peatlands with the smallest WT temporal fluctuations. Similarly, we obtained a weak relationship ($R = 0.4$ between WT and OPTRAM_NDVI) at site 101, even though its "best pixel" had 0% tree coverage. Peatland 101 had shallow (often above the surface) and stable WT (Table S1). This finding also agrees with a result by Lees et al. (2020), showing a missing relationship between a SWIR-based moisture index and WT under a limited range of high water content.

4.3. The potential of OPTRAM in studying restored peatlands

Our results suggest that OPTRAM can be used to monitor WT dynamics in both restored and intact peatlands (Fig. 4). We observed moderate to high values of long-term anomaly correlation between WT and OPTRAM estimates. The short-term anomaly correlation values were lower, probably because short-term anomalies are more strongly impacted by noise in the data. Nevertheless, short-term anomaly correlations for intact and restored peatlands were comparable.

Meanwhile, a previous study that utilised the same dataset with restored peatlands found that the average performance of regression with OPTRAM was worse for restored peatlands than for intact ones (Räsänen et al., 2022). Räsänen et al. (2022) did not use the "best pixel" approach; instead, they used OPTRAM estimates from the pixels near the monitoring wells. Therefore, we assume that the comparatively weaker performance of OPTRAM in Räsänen et al. (2022) could be due to the higher tree coverage of restored peatlands that were previously used for forestry.

In many restored sites, OPTRAM yielded high correlation values that were comparable with correlation values in intact sites (Fig. 4). We used data from 23 restored peatlands, and fourteen of them had 0% tree cover density of the "best pixels". Among these peatlands was site 101, with a stable shallow WT and site 45, with a statistically significant breaking point in WT and OPTRAM_NDVI relationships. Excluding sites 101 and 45, correlation values for the rest varied from −0.1 to 0.9 (median 0.6). Also, there is no ground to conclude better OPTRAM performance over the intact than restored sites based on short-term anomaly correlation (Fig. 4). For example, restored oligotrophic peatlands resulted in similar short-term anomaly correlation values to intact oligotrophic peatlands. Future research should investigate long-term anomaly correlation in restored peatlands, which, unfortunately, was impossible in our study.

4.4. Future research directions

Our study has shown that OPTRAM has the potential to be used at a large scale for monitoring WT dynamics in northern peatlands. Out of 53 studied peatlands, 20 peatlands had high R ($R > 0.7$) between OPTRAM_NDVI and WT. Among those 20 peatlands, 14 were intact, and six were restored. Though this is a promising result, OPTRAM has several drawbacks and limitations that should be addressed in future research.

First, our algorithm could not reliably detect the wet and dry edges for the sites with less than 25,000 total pixels. In our study, we aimed to estimate the dry and wet edges of OPTRAM using automated parametrisation in a cloud-based platform GEE instead of classical visual parametrisation (Babaeian et al., 2019; Räsänen et al., 2022; Sadeghi et al., 2017). An automated parametrisation enables a global-scale application of OPTRAM in the future. The limitation of having at least 25,000 total pixels might be overcome in future work by creating one NDVI-STR space for several small peatlands with similar vegetation cover. Thus, one set of dry and wet edges can be estimated since the same plant species have similar reflectance properties disregarding the location of the peatland where plants were sampled (Bubier et al., 1997; Salko et al., 2023).

Second, future work could also focus on studying the breaking point between WT and OPTRAM relationships caused by vegetation water stress. Vegetation responds to water stress through changes in biochemistry and pigments (Gerhards et al., 2019), which could be detected with new hyperspectral satellite missions, e.g., EnMAP (Guanter et al., 2015) and PRISMA (Loizzo et al., 2018). Utilising hyperspectral data along with OPTRAM has potential to reveal indicators of vegetation water stress, after which the breaking point occurs. Identification of the breaking point after which OPTRAM loses sensitivity to WT will make OPTRAM application more robust and allow a combination of OPTRAM with backscatter data for monitoring WT in peatlands under a wide range of moisture conditions (Bechtold et al., 2018).

Finally, after the challenges associated with automated parametrisation and breaking point between WT and OPTRAM relationships will be solved, OPTRAM estimates can be potentially assimilated into land surface models as a proxy of moisture conditions over the northern peatlands (De Lannoy et al., 2022). Despite the critical role of peatlands in the carbon cycle, land surface models only recently started accounting for these carbon-rich soils (Vereecken et al., 2022). One such land surface model is PEAT-CLSM (Bechtold et al., 2019), and it can be expected that OPTRAM can add value to these models in a similar way as earlier studies have shown by assimilating much coarser passive microwave observations (~40 km) (Bechtold et al., 2020; Reichle et al., 2023). The assimilation of OPTRAM information of much higher spatial resolution could render such data assimilation products appropriate for peatland management applications. At the same time, the use of a land surface model will be beneficial for global OPTRAM applications because model-simulated WT estimates can be used to derive the peatland-specific relationships between OPTRAM and WT (Burdun et al., 2020b). This, in turn, enables the identification of a "best pixel" in peatlands with no in-situ WT data.

5. Conclusions

Our investigation on the potential and pitfalls of OPTRAM for monitoring WT in northern peatlands strengthened the idea that OPTRAM can detect temporal interannual variability of WT in intact and restored (previously forestry-drained) peatlands with low tree coverage. The findings of our study are as follows:

1. The choice of vegetation index used in OPTRAM does not significantly affect OPTRAM performance. Four OPTRAM estimates based

on four vegetation indices (NDVI, kNDVI, EVI, RENDVI) result in similar correlation and anomaly correlation metrics with in situ WT.
2. The tree cover density decreases the sensitivity of OPTRAM to WT. For the pixels with tree cover density greater than 50%, the correlation between WT and OPTRAM_NDVI decreases.
3. OPTRAM seems to be in particular suitable to monitor long-term (i.e., interannual) WT variability while performance for short-term changes (e.g., response to individual rain events) was lower.
4. The relationship between WT and OPTRAM can vanish when WT gets deeper.
5. OPTRAM fails to detect WT dynamics in peatlands with shallow and stable WT and in drained peatlands with deep WT.

Our findings suggest that OPTRAM can be used to monitor temporal dynamics in northern restored and intact peatlands with low tree cover density (below 50%). Keeping in mind the limitations of OPTRAM, further research should explore the utility of OPTRAM for monitoring peatlands processes connected to moisture conditions, e.g., greenhouse gas emissions, peat fires, and ecological resilience to climate change.

CRediT authorship contribution statement

Iuliia Burdun: Conceptualization, Methodology, Software, Validation, Formal analysis, Data curation, Writing – original draft, Visualization. **Michel Bechtold:** Conceptualization, Formal analysis, Writing – review & editing, Supervision. **Mika Aurela:** Writing – review & editing, Data curation. **Gabrielle De Lannoy:** Writing – review & editing. **Ankur R. Desai:** Writing – review & editing, Data curation. **Elyn Humphreys:** Writing – review & editing, Data curation. **Santtu Kareksela:** Writing – review & editing, Data curation. **Viacheslav Komisarenko:** Methodology, Software. **Maarit Liimatainen:** Writing – review & editing, Data curation. **Hannu Marttila:** Writing – review & editing, Data curation. **Kari Minkkinen:** Writing – review & editing, Data curation. **Mats B. Nilsson:** Writing – review & editing, Data curation. **Paavo Ojanen:** Writing – review & editing, Data curation. **Sini-Selina Salko:** Writing – review & editing, Data curation. **Eeva-Stiina Tuittila:** Writing – review & editing, Data curation. **Evelyn Uuemaa:** Writing – review & editing, Data curation. **Miina Rautiainen:** Conceptualization, Methodology, Resources, Data curation, Writing – review & editing, Supervision, Project administration, Funding acquisition.

Declaration of Competing Interest

The authors declare that they have no known competing financial interests or personal relationships that could have appeared to influence the work reported in this paper.

Data availability

Sentinel-2 data are available at https://developers.google.com/earth-engine/datasets/catalog/COPERNICUS_S2_SR_HARMONIZED. The in situ WT datasets are available from the authors upon request. Code in Google Earth Engine to calculate OPTRAM_NDVI parameters for wet edge https://code.earthengine.google.com/a2c93798f27835b48d2efb300ebbb2e9?noload=true and dry edge https://code.earthengine.google.com/2887c0bad9558d579eb7b5c6296a1a89?noload=true in EE_MAN peatland.

Acknowledgements

This study was mainly funded by the Academy of Finland (PEATSPEC, decision no 341963). This study has also received funding from the European Research Council (ERC) under the European Union's Horizon 2020 research and innovation programme (grant agreement No 771049, MR). The text reflects only the authors' view, and the Agency is not responsible for any use that may be made of the information it contains. We thank the Estonian Weather Service for providing us with the data for EE_MAN and EE_LIN peatlands. ARD acknowledge support for US-Los from the US Department of Energy Ameriflux Network Management Project. EU was funded by Estonian Research Agency's grant no. PRG1764. HM acknowledged support for the Pallas site from Maa- ja Vesitekniikan tuki ry, Academy of Finland (grants 347704, 346163, 347663) and Freshwater competence centre. ML acknowledges support for Ruukki site from the Centre for Economic Development, Transport and the Environment, Ministry of Agriculture and Forestry of Finland, Niemi foundation, Suoviljelysyhdistys and Kone Foundation. MB acknowledges funding from the Research Foundation - Flanders (FWO) (FWO.G095720N). EST acknowledge support from Academy of Finland Flagship funding for ACCC (grant No. 337550) and for the BorPeat project (330840) and infrastructure (337064, 345527). SK's work and the Finnish peatland restoration monitoring network were funded by the Finnish Ministry of the Environment. CA-MER research was conducted with logistical support from the National Capital Commission and financial support from the Ontario Ministry of Environment, Conservation and Parks. We express our gratitude to the anonymous reviewers who helped us to improve the clarity, precision, and relevance of the article.

Appendix A. Dry and wet edge estimation

To estimate the dry and wet edges, we divided the vegetation indices' ranges into intervals with a step of 0.001 and each interval into ten subintervals. First, we identified the maximal (STR_{max}) STR values within each subinterval for the wet edge. Second, we estimated each interval's median (STR_{median}) and standard deviations (STR_{sd}) of STR_{max}. Within each interval, we filtered out STR_{max} greater than the sum of STR_{median} and STR_{sd} for this interval. Third, within each interval, we calculated median values of the remained STR_{max} and their NDVI; these were the $STR_{max,}$ and NDVI values used to fit the linear regression for wet edge calculation. Fourth, we fit the linear regression for the wet edge and estimated its *Root-Mean-Square Error* (*RMSE*). If the interval's STR_{max} value was greater than the doubled RMSE, this interval was further excluded, and linear regression was fitted again. Fifth, the slope (s_{max}) and intercept (int_{max}) of the wet edge were finally calculated and exported from GEE for further OPTRAM estimation in R software. Similar steps were repeated with the minimal (STR_{min}) STR values for the dry edge estimation.

Appendix B. Supplementary data

Supplementary data to this article can be found online at https://doi.org/10.1016/j.rse.2023.113736.

References

Ambrosone, M., Matese, A., Di Gennaro, S.F., Gioli, B., Tudoroiu, M., Genesio, L., Miglietta, F., Baronti, S., Maienza, A., Ungaro, F., Toscano, P., 2020. Retrieving soil moisture in rainfed and irrigated fields using Sentinel-2 observations and a modified OPTRAM approach. Int. J. Appl. Earth Obs. Geoinf. 89, 102113 https://doi.org/10.1016/j.jag.2020.102113.

Arroyo-Mora, J.P., Kalacska, M., Soffer, R., Ifimov, G., Leblanc, G., Schaaf, E.S., Lucanus, O., 2018. Evaluation of phenospectral dynamics with Sentinel-2A using a bottom-up approach in a northern ombrotrophic peatland. Remote Sens. Environ. 216, 544–560. https://doi.org/10.1016/J.RSE.2018.07.021.

Asmuß, T., Bechtold, M., Tiemeyer, B., 2019. On the potential of Sentinel-1 for high resolution monitoring of water table dynamics in grasslands on organic soils. Remote Sens. 11, 1659. https://doi.org/10.3390/rs11141659.

Babaeian, E., Sadeghi, M., Franz, T.E., Jones, S., Tuller, M., 2018. Mapping soil moisture with the OPtical TRApezoid model (OPTRAM) based on long-term MODIS observations. Remote Sens. Environ. 211, 425–440. https://doi.org/10.1016/j.rse.2018.04.029.

Babaeian, E., Sidike, P., Newcomb, M.S., Maimaitijiang, M., White, S.A., Demieville, J., Ward, R.W., Sadeghi, M., LeBauer, D.S., Jones, S.B., Sagan, V., Tuller, M., 2019. A new optical remote sensing technique for high-resolution mapping of soil moisture. Front. Big Data 2, 37. https://doi.org/10.3389/fdata.2019.00037.

Banskota, A., Falkowski, M.J., Smith, A.M.S., Kane, E.S., Meingast, K.M., Bourgeau-Chavez, L.L., Miller, M.E., French, N.H., 2017. Continuous wavelet analysis for

spectroscopic determination of subsurface moisture and water-table height in northern peatland ecosystems. IEEE Trans. Geosci. Remote Sens. 55, 1526–1536. https://doi.org/10.1109/TGRS.2016.2626460.

Bechtold, M., Schlaffer, S., Tiemeyer, B., De Lannoy, G., 2018. Inferring water table depth dynamics from ENVISAT-ASAR C-band backscatter over a range of peatlands from deeply-drained to natural conditions. Remote Sens. 10, 536. https://doi.org/10.3390/rs10040536.

Bechtold, M., De Lannoy, G., Koster, R.D., Reichle, R.H., Mahanama, S., Bleuten, W., Bourgault, M.A., Brümmer, C., Burdun, I., Desai, A.R., Devito, K., Grünwald, T., Grygoruk, M., Humphreys, E.R., Klatt, J., Kurbatova, J., Lohila, A., Munir, T.M., Nilsson, M.B., Price, J.S., Röhl, M., Schneider, A., Tiemeyer, B., 2019. PEAT-CLSM: a specific treatment of peatland hydrology in the NASA catchment land surface model. J. Adv. Model. Earth Syst. 11, 1–33. https://doi.org/10.1029/2018MS001574.

Bechtold, M., De Lannoy, G., Reichle, R.H., Roose, D., Balliston, N., Burdun, I., Devito, K., Kurbatova, J., Munir, T.M., Zarov, E.A., 2020. Improved groundwater table and L-band brightness temperature estimates for northern hemisphere peatlands using new model physics and SMOS observations in a global data assimilation framework. Remote Sens. Environ. 246, 1–10. https://doi.org/10.1016/j.rse.2020.111805.

Bryant, R.G., Baird, A.J., 2003. The spectral behaviour of *Sphagnum* canopies under varying hydrological conditions. Geophys. Res. Lett. 30, 1134. https://doi.org/10.1029/2002GL016053.

Bubier, J.L., Rock, B.N., Crill, P.M., 1997. Spectral reflectance measurements of boreal wetland and forest mosses. J. Geophys. Res. Atmos. 102, 29483–29494. https://doi.org/10.1029/97JD02316.

Burdun, I., Sagris, V., Mander, Ü., 2019. Relationships between field-measured hydrometeorological variables and satellite-based land surface temperature in a hemiboreal raised bog. Int. J. Appl. Earth Obs. Geoinf. 74, 295–301. https://doi.org/10.1016/j.jag.2018.09.019.

Burdun, I., Bechtold, M., Sagris, V., Komisarenko, V., De Lannoy, G., Mander, Ü., 2020a. A comparison of three trapezoid models using optical and thermal satellite imagery for water table depth monitoring in Estonian bogs. Remote Sens. 12, 1–24. https://doi.org/10.3390/rs12121980.

Burdun, I., Bechtold, M., Sagris, V., Lohila, A., Humphreys, E., Desai, A.R., Nilsson, M.B., De Lannoy, G., Mander, Ü., 2020b. Satellite determination of peatland water table temporal dynamics by localizing representative pixels of a SWIR-based moisture index. Remote Sens. 12, 1–21. https://doi.org/10.3390/rs12182936.

Camps-Valls, G., Campos-Taberner, M., Moreno-Martínez, Á., Walther, S., Duveiller, G., Cescatti, A., Mahecha, M.D., Muñoz-Marí, J., García-Haro, F.J., Guanter, L., Jung, M., Gamon, J.A., Reichstein, M., Running, S.W., 2021. A unified vegetation index for quantifying the terrestrial biosphere. Sci. Adv. 7, 7447–7473. https://doi.org/10.1126/SCIADV.ABC7447/SUPPL_FILE/ABC7447_SM.PDF.

Carlson, T., 2007. An overview of the "triangle method" for estimating surface evapotranspiration and soil moisture from satellite imagery. Sensors 7, 1612–1629. https://doi.org/10.3390/s7081612.

Chaudhary, N., Westermann, S., Lamba, S., Shurpali, N., Sannel, A.B.K., Schurgers, G., Miller, P.A., Smith, B., 2020. Modelling past and future peatland carbon dynamics across the pan-Arctic. Glob. Chang. Biol. 26, 4119–4133. https://doi.org/10.1111/GCB.15099.

Chen, M., Zhang, Y., Yao, Y., Lu, J., Pu, X., Hu, T., Wang, P., 2020. Evaluation of an OPtical TRApezoid Model (OPTRAM) to retrieve soil moisture in the Sanjiang Plain of Northeast China. Earth Sp. Sci. https://doi.org/10.1029/2020EA001108.

D'Acunha, B., Lee, S.C., Johnson, M.S., 2018. Ecohydrological responses to rewetting of a highly impacted raised bog ecosystem. Ecohydrology 11. https://doi.org/10.1002/ECO.1922.

De Lannoy, G.J.M., Bechtold, M., Albergel, C., Brocca, L., Calvet, J.-C., Carrassi, A., Crow, W.T., de Rosnay, P., Durand, M., Forman, B., Geppert, G., Girotto, M., Hendricks Franssen, H.-J., Jonas, T., Kumar, S., Lievens, H., Lu, Y., Massari, C., Pauwels, V.R.N., Reichle, R.H., Steele-Dunne, S., 2022. Perspective on satellite-based land data assimilation to estimate water cycle components in an era of advanced data availability and model sophistication. Front. Water 4, 156. https://doi.org/10.3389/FRWA.2022.981745.

Defries, R.S., Townshend, J.R., 2007. NDVI-derived land cover classifications at a global scale. Int. J. Remote Sens. 15, 3567–3586. https://doi.org/10.1080/01431169408954345.

Dooley, K., Nicholls, Z., Meinshausen, M., 2022. Carbon removals from nature restoration are no substitute for steep emission reductions. One Earth 5, 812–824. https://doi.org/10.1016/J.ONEEAR.2022.06.002.

European Environment Agency, 2018. High Resolution Layer: Tree Cover Density (TCD) 2018 [WWW Document]. https://land.copernicus.eu/pan-european/high-resolution-layers/forests/tree-cover-density/status-maps/tree-cover-density-2018?tab=metadata (accessed 9.27.22).

European Space Agency, 2015. SENTINEL-2 User Handbook. ESA Standard Document.

Farooq, M., Wahid, A., Kobayashi, N., Fujita, D., Basra, S.M.A., 2009. Plant drought stress: effects, mechanisms and management. Sustain. Agric. 153–188 https://doi.org/10.1007/978-90-481-2666-8_12/COVER.

Forsström, P., Peltoniemi, J., Rautiainen, M., 2019. Seasonal dynamics of lingonberry and blueberry spectra. Silva Fenn. 53 https://doi.org/10.14214/SF.10150.

Forzieri, G., Dakos, V., McDowell, N.G., Ramdane, A., Cescatti, A., 2022. Emerging signals of declining forest resilience under climate change. Nat 6087923 (608), 534–539. https://doi.org/10.1038/s41586-022-04959-9.

Gallant, A.L., 2015. The challenges of remote monitoring of wetlands. Remote Sens. 7, 10938–10950. https://doi.org/10.3390/RS70810938.

Gao, B.C., 1996. NDWI—a normalized difference water index for remote sensing of vegetation liquid water from space. Remote Sens. Environ. 58, 257–266. https://doi.org/10.1016/S0034-4257(96)00067-3.

Gerhards, M., Schlerf, M., Mallick, K., Udelhoven, T., 2019. Challenges and future perspectives of multi-/hyperspectral thermal infrared remote sensing for crop water-stress detection: a review. Remote Sens. 11 https://doi.org/10.3390/RS11101240, 1240 11.

Gitelson, A., Merzlyak, M.N., 1994. Spectral reflectance changes associated with autumn senescence of Aesculus hippocastanum L. and Acer platanoides L. leaves. spectral features and relation to chlorophyll estimation. J. Plant Physiol. 143, 286–292. https://doi.org/10.1016/S0176-1617(11)81633-0.

Gong, J., Roulet, N., Frolking, S., Peltola, H., Laine, A.M., Kokkonen, N., Tuittila, E.S., 2020. Modelling the habitat preference of two key Sphagnum species in a poor fen as controlled by capitulum water content. Biogeosciences 17, 5693–5719. https://doi.org/10.5194/BG-17-5693-2020.

Gorelick, N., Hancher, M., Dixon, M., Ilyushchenko, S., Thau, D., Moore, R., 2017. Google Earth Engine: planetary-scale geospatial analysis for everyone. Remote Sens. Environ. 202, 18–27. https://doi.org/10.1016/j.rse.2017.06.031.

Guanter, L., Kaufmann, H., Segl, K., Foerster, S., Rogass, C., Chabrillat, S., Kuester, T., Hollstein, A., Rossner, G., Chlebek, C., Straif, C., Fischer, S., Schrader, S., Storch, T., Heiden, U., Mueller, A., Bachmann, M., Mühle, H., Müller, R., Habermeyer, M., Ohndorf, A., Hill, J., Buddenbaum, H., Hostert, P., Van Der Linden, S., Leitão, P.J., Rabe, A., Doerffer, R., Krasemann, H., Xi, H., Mauser, W., Hank, T., Locherer, M., Rast, M., Staenz, K., Sang, B., 2015. The EnMAP spaceborne imaging spectroscopy mission for earth observation. Remote Sens. 7, 8830–8857. https://doi.org/10.3390/RS70708830.

Hadi, Korhonen, L., Hovi, A., Rönnholm, P., Rautiainen, M., 2016. The accuracy of large-area forest canopy cover estimation using Landsat in boreal region. Int. J. Appl. Earth Obs. Geoinf. 53, 118–127. https://doi.org/10.1016/J.JAG.2016.08.009.

Harris, A., Bryant, R.G., 2009. A multi-scale remote sensing approach for monitoring northern peatland hydrology: present possibilities and future challenges. J. Environ. Manag. 90, 2178–2188. https://doi.org/10.1016/j.jenvman.2007.06.025.

Harris, A., Bryant, R.G., Baird, A.J., 2005. Detecting near-surface moisture stress in Sphagnum spp. Remote Sens. Environ. 97, 371–381. https://doi.org/10.1016/J.RSE.2005.05.001.

Harris, A., Bryant, R.G.G., Baird, A.J.J., 2006. Mapping the effects of water stress on Sphagnum: preliminary observations using airborne remote sensing. Remote Sens. Environ. 100, 363–378. https://doi.org/10.1016/J.RSE.2005.10.024.

Helbig, M., Živković, T., Alekseychik, P., Aurela, M., El-Madany, T.S., Euskirchen, E.S., Flanagan, L.B., Griffis, T.J., Hanson, P.J., Hattakka, J., Helfter, C., Hirano, T., Humphreys, E.R., Kiely, G., Kolka, R.K., Laurila, T., Leahy, P.G., Lohila, A., Mammarella, I., Nilsson, M.B., Panov, A., Parmentier, F.J.W., Peichl, M., Rinne, J., Roman, D.T., Sonnentag, O., Tuittila, E.S., Ueyama, M., Vesala, T., Vestin, P., Weldon, S., Weslien, P., Zaehle, S., 2022. Warming response of peatland CO2 sink is sensitive to seasonality in warming trends. Nat. Clim. Chang. 128 (12), 743–749. https://doi.org/10.1038/s41558-022-01428-z.

Hirschler, O., Osterburg, B., 2022. Peat extraction, trade and use in Europe: a material flow analysis. Mires Peat 24–27. https://doi.org/10.19189/MaP.2021.SNPG.StA.2315.

Hokanson, K.J., Moore, P.A., Lukenbach, M.C., Devito, K.J., Kettridge, N., Petrone, R.M., Mendoza, C.A., Waddington, J.M., 2018. A hydrogeological landscape framework to identify peatland wildfire smouldering hot spots. Ecohydrology 11. https://doi.org/10.1002/eco.1942.

Howie, S.A., van Meerveld, H.J., 2013. Regional and local patterns in depth to water table, hydrochemistry and peat properties of bogs and their laggs in coastal British Columbia. Hydrol. Earth Syst. Sci. 17, 3421–3435. https://doi.org/10.5194/hess-17-3421-2013.

Huang, Y., Ciais, P., Luo, Y., Zhu, D., Wang, Y., Qiu, C., Goll, D.S., Guenet, B., Makowski, D., De Graaf, I., Leifeld, J., Kwon, M.J., Hu, J., Qu, L., 2021. Tradeoff of CO2 and CH4 emissions from global peatlands under water-table drawdown. Nat. Clim. Chang. 117 (11), 618–622. https://doi.org/10.1038/s41558-021-01059-w.

Huete, A.R., 1988. A soil-adjusted vegetation index (SAVI). Remote Sens. Environ. 25, 295–309. https://doi.org/10.1016/0034-4257(88)90106-X.

Huete, A., Didan, K., Miura, T., Rodriguez, E., Gao, X., Ferreira, L., 2002. Overview of the radiometric and biophysical performance of the MODIS vegetation indices. Remote Sens. Environ. 83, 195–213. https://doi.org/10.1016/S0034-4257(02)00096-2.

Justice, C.O., Markham, B.L., Townshend, J.R., Kennard, R.L., 2007. Spatial degradation of satellite data. Int. J. Remote Sens. 10, 1539–1561. https://doi.org/10.1080/01431168908903989.

Kalacska, M., Lalonde, M., Moore, T.R., 2015. Estimation of foliar chlorophyll and nitrogen content in an ombrotrophic bog from hyperspectral data: scaling from leaf to image. Remote Sens. Environ. 169, 270–279. https://doi.org/10.1016/J.RSE.2015.08.012.

Kalacska, M., Arroyo-Mora, J., Soffer, R., Roulet, N., Moore, T., Humphreys, E., Leblanc, G., Lucanus, O., Inamdar, D., 2018. Estimating peatland water table depth and net ecosystem exchange: a comparison between satellite and airborne imagery. Remote Sens. 10, 687. https://doi.org/10.3390/rs10050687.

Kreyling, J., Tanneberger, F., Jansen, F., van der Linden, S., Aggenbach, C., Blüml, V., Couwenberg, J., Emsens, W.J., Joosten, H., Klimkowska, A., Kotowski, W., Kozub, L., Lennartz, B., Liczner, Y., Liu, H., Michaelis, D., Oehmke, C., Parakenings, K., Pleyl, E., Poyda, A., Raabe, S., Röhl, M., Rücker, K., Schneider, A., Schrautzer, J., Schröder, C., Schug, F., Seeber, E., Thiel, F., Thiele, S., Tiemeyer, B., Timmermann, T., Urich, T., van Diggelen, R., Vegelin, K., Verbruggen, E., Wilmking, M., Wrage-Mönnig, N., Wołejko, L., Zak, D., Jurasinski, G., 2021. Rewetting does not return drained fen peatlands to their old selves. Nat. Commun. 121 (12), 1–8. https://doi.org/10.1038/s41467-021-25619-y.

Kwon, M.J., Ballantyne, A., Ciais, P., Qiu, C., Salmon, E., Raoult, N., Guenet, B., Göckede, M., Euskirchen, E.S., Nykänen, H., Schuur, E.A.G., Turetsky, M.R., Dieleman, C.M., Kane, E.S., Zona, D., 2022. Lowering water table reduces carbon

sink strength and carbon stocks in northern peatlands. Glob. Chang. Biol. 00, 1–19. https://doi.org/10.1111/GCB.16394.
Laine, Anna M., Mäkiranta, P., Laiho, R., Mehtätalo, L., Penttilä, T., Korrensalo, A., Minkkinen, K., Fritze, H., Tuittila, E.S., 2019a. Warming impacts on boreal fen CO2 exchange under wet and dry conditions. Glob. Chang. Biol. 25, 1995–2008. https://doi.org/10.1111/GCB.14617.
Laine, A.M., Mehtätalo, L., Tolvanen, A., Frolking, S., Tuittila, E.S., 2019b. Impacts of drainage, restoration and warming on boreal wetland greenhouse gas fluxes. Sci. Total Environ. 647, 169–181. https://doi.org/10.1016/J.SCITOTENV.2018.07.390.
Laio, F., Porporato, A., Fernandez-Illescas, C.P., Rodriguez-Iturbe, I., 2001. Plants in water-controlled ecosystems: active role in hydrologic processes and response to water stress: IV. Discussion of real cases. Adv. Water Resour. 24, 745–762. https://doi.org/10.1016/S0309-1708(01)00007-0.
Lees, K.J., Lees, K.J., Artz, R.R.E., Khomik, M., Clark, J.M., Ritson, J., Hancock, M.H., Cowie, N.R., Quaife, T., 2020. Using spectral indices to estimate water content and GPP in sphagnum moss and other peatland vegetation. IEEE Trans. Geosci. Remote Sens. 58, 4547–4557. https://doi.org/10.1109/TGRS.2019.2961479.
Lees, K.J., Artz, R.R.E., Chandler, D., Aspinall, T., Boulton, C.A., Buxton, J., Cowie, N.R., Lenton, T.M., 2021. Using remote sensing to assess peatland resilience by estimating soil surface moisture and drought recovery. Sci. Total Environ. 761, 143312 https://doi.org/10.1016/J.SCITOTENV.2020.143312.
Leifeld, J., Menichetti, L., 2018. The underappreciated potential of peatlands in global climate change mitigation strategies. Nat. Commun. 9, 1–7. https://doi.org/10.1038/s41467-018-03406-6.
Leifeld, J., Wüst-Galley, C., Page, S., 2019. Intact and managed peatland soils as a source and sink of GHGs from 1850 to 2100. Nat. Clim. Chang. https://doi.org/10.1038/s41558-019-0615-5.
Letts, M.G., Comer, N.T., Roulet, N.T., Skarupa, M.R., Verseghy, D.L., 2000. Parametrization of peatland hydraulic properties for the Canadian land surface scheme. Atmosphere-Ocean 38, 141–160. https://doi.org/10.1080/07055900.2000.9649643.
Liu, H., Price, J., Rezanezhad, F., Lennartz, B., 2020. Centennial-scale shifts in hydrophysical properties of peat induced by drainage. Water Resour. Res. 56 https://doi.org/10.1029/2020WR027538 e2020WR027538.
Loisel, J., Gallego-Sala, A., 2022. Ecological resilience of restored peatlands to climate change. Commun. Earth Environ 31 (3), 1–8. https://doi.org/10.1038/s43247-022-00547-x.
Loisel, J., Gallego-Sala, A.V., Amesbury, M.J., Magnan, G., Anshari, G., Beilman, D.W., Benavides, J.C., Blewett, J., Camill, P., Charman, D.J., Chawchai, S., Hedgpeth, A., Kleinen, T., Korhola, A., Large, D., Mansilla, C.A., Müller, J., van Bellen, S., West, J. B., Yu, Z., Bubier, J.L., Garneau, M., Moore, T., Sannel, A.B.K., Page, S., Väliranta, M., Bechtold, M., Brovkin, V., Cole, L.E.S., Chanton, J.P., Christensen, T. R., Davies, M.A., De Vleeschouwer, F., Finkelstein, S.A., Frolking, S., Gałka, M., Gandois, L., Girkin, N., Harris, L.I., Heinemeyer, A., Hoyt, A.M., Jones, M.C., Joos, F., Juutinen, S., Kaiser, K., Lacourse, T., Lamentowicz, M., Larmola, T., Leifeld, J., Lohila, A., Milner, A.M., Minkkinen, K., Moss, P., Naafs, B.D.A., Nichols, J., O'Donnell, J., Payne, R., Philben, M., Piilo, S., Quillet, A., Ratnayake, A. S., Roland, T.P., Sjögersten, S., Sonnentag, O., Swindles, G.T., Swinnen, W., Talbot, J., Treat, C., Valach, A.C., Wu, J., 2021. Expert assessment of future vulnerability of the global peatland carbon sink. Nat. Clim. Chang. 11, 70–77. https://doi.org/10.1038/s41558-020-00944-0.
Loizzo, R., Guarini, R., Longo, F., Scopa, T., Formaro, R., Facchinetti, C., Varacalli, G., 2018. Prisma: The Italian hyperspectral mission. Int. Geosci. Remote Sens. Symp. 2018-July, pp. 175–178. https://doi.org/10.1109/IGARSS.2018.8518512.
Malhotra, A., Roulet, N.T., Wilson, P., Giroux-Bougard, X., Harris, L.I., 2016. Ecohydrological feedbacks in peatlands: an empirical test of the relationship among vegetation, microtopography and water table. Ecohydrology 9, 1346–1357. https://doi.org/10.1002/eco.1731.
Meingast, K.M., Falkowski, M.J., Kane, E.S., Potvin, L.R., Benscoter, B.W., Smith, A.M.S., Bourgeau-Chavez, L.L., Miller, M.E., 2014. Spectral detection of near-surface moisture content and water-table position in northern peatland ecosystems. Remote Sens. Environ. 152, 536–546. https://doi.org/10.1016/J.RSE.2014.07.014.
Melton, J.R., Chan, E., Millard, K., Fortier, M., Winton, R.S., Martín-López, J.M., Cadillo-Quiroz, H., Kidd, D., Verchot, L.V., 2022. A map of global peatland extent created using machine learning (Peat-ML). Geosci. Model Dev. 15, 4709–4738. https://doi.org/10.5194/GMD-15-4709-2022.
Menberu, M.W., Tahvanainen, T., Marttila, H., Irannezhad, M., Ronkanen, A.K., Penttinen, J., Kløve, B., 2016. Water-table-dependent hydrological changes following peatland forestry drainage and restoration: analysis of restoration success. Water Resour. Res. 52, 3742–3760. https://doi.org/10.1002/2015WR018578.
Menberu, M.W., Haghighi, A.T., Ronkanen, A.K., Marttila, H., Kløve, B., 2018. Effects of drainage and subsequent restoration on peatland hydrological processes at catchment scale. Water Resour. Res. 54, 4479–4497. https://doi.org/10.1029/2017WR022362.
Millar, D.J., Cooper, D.J., Dwire, K.A., Hubbard, R.M., Ronayne, M.J., von Fischer, J., David Millar, C.J., 2023. Hydrological dynamics and associated greenhouse gas fluxes in a mountain peatland under different climate scenarios. Ecohydrology e2536. https://doi.org/10.1002/ECO.2536.
Mokhtari, A., Sadeghi, M., Afrasiabian, Y., Yu, K., 2023. OPTRAM-ET: a novel approach to remote sensing of actual evapotranspiration applied to Sentinel-2 and Landsat-8 observations. Remote Sens. Environ. 286, 113443 https://doi.org/10.1016/J.RSE.2022.113443.
Pablo Arroyo-Mora, J., Kalacska, M., Lucanus, O., Soffer, R., Leblanc Pablo Arroyo-Mora, G.J., Leblanc, G., 2017. Spectro-spatial relationship between UAV derived high resolution DEM and SWIR hyperspectral data: application to an ombrotrophic peatland. Remote Sens. Agric. Ecosyst. Hydrol. 10421, 131–142. https://doi.org/10.1117/12.2277874.
Peichl, M., Öquist, M., Ottosson Löfvenius, M., Ilstedt, U., Sagerfors, J., Grelle, A., Lindroth, A., Nilsson, M.B., 2014. A 12-year record reveals pre-growing season temperature and water table level threshold effects on the net carbon dioxide exchange in a boreal fen. Environ. Res. Lett. 9, 055006 https://doi.org/10.1088/1748-9326/9/5/055006.
Potvin, L.R., Kane, E.S., Chimner, R.A., Kolka, R.K., Lilleskov, E.A., 2015. Effects of water table position and plant functional group on plant community, aboveground production, and peat properties in a peatland mesocosm experiment (PEATcosm). Plant Soil 387, 277–294. https://doi.org/10.1007/S11104-014-2301-8/FIGURES/7.
Qiu, C., Zhu, D., Ciais, P., Guenet, B., Peng, S., 2020. The role of northern peatlands in the global carbon cycle for the 21st century. Glob. Ecol. Biogeogr. 29, 956–973. https://doi.org/10.1111/GEB.13081.
Qiu, C., Ciais, P., Zhu, D., Guenet, B., Chang, J., Chaudhary, N., Kleinen, T., Li, X.Y., Müller, J., Xi, Y., Zhang, W., Ballantyne, A., Brewer, S.C., Brovkin, V., Charman, D.J., Gustafson, A., Gallego-Sala, A.V., Gasser, T., Holden, J., Joos, F., Kwon, M.J., Lauerwald, R., Miller, P.A., Peng, S., Page, S., Smith, B., Stocker, B.D., Sannel, A.B.K., Salmon, E., Schurgers, G., Shurpali, N.J., Wårlind, D., Westermann, S., 2022. A strong mitigation scenario maintains climate neutrality of northern peatlands. One Earth 5, 86–97. https://doi.org/10.1016/j.oneear.2021.12.008.
R Core Team, 2022. R: A Language and Environment for Statistical Computing.
Rantanen, M., Karpechko, A.Y., Lipponen, A., Nordling, K., Hyvärinen, O., Ruosteenoja, K., Vihma, T., Laaksonen, A., 2022. The Arctic has warmed nearly four times faster than the globe since 1979. Commun. Earth Environ 31 (3), 1–10. https://doi.org/10.1038/s43247-022-00498-3.
Räsänen, A., Tolvanen, A., Kareksela, S., 2022. Monitoring peatland water table depth with optical and radar satellite imagery. Int. J. Appl. Earth Obs. Geoinf. 112, 102866 https://doi.org/10.1016/J.JAG.2022.102866.
Reichle, R.H., Liu, Q., Ardizzone, J.V., Bechtold, M., Crow, W.T., Lannoy, G.J.M.D., Kimball, J.S., Koster, R.D., 2023. Soil Moisture Active Passive (SMAP) Project Assessment Report for Version 7 of the L4_SM Data Product. Maryland, USA.
Rice, S.K., Aclander, L., Hanson, D.T., 2008. Do bryophyte shoot systems function like vascular plant leaves or canopies? Functional trait relationships in Sphagnum mosses (Sphagnaceae). Am. J. Bot. 95, 1366–1374. https://doi.org/10.3732/AJB.0800019.
Rouse, J., Haas, J., Schell, J., Deering, D., 1973. Monitoring vegetation systems in the great plains with ERTS. Third ERTS Symp. 1, 309–317.
Sadeghi, M., Jones, S.B., Philpot, W.D., 2015. A linear physically-based model for remote sensing of soil moisture using short wave infrared bands. Remote Sens. Environ. 164, 66–76. https://doi.org/10.1016/j.rse.2015.04.007.
Sadeghi, M., Babaeian, E., Tuller, M., Jones, S.B., 2017. The optical trapezoid model: a novel approach to remote sensing of soil moisture applied to Sentinel-2 and Landsat-8 observations. Remote Sens. Environ. 198, 52–68. https://doi.org/10.1016/J.RSE.2017.05.041.
Salko, S.-S., Juola, Jussi, Burdun, I., Vasander, H., Rautiainen, M., 2023. Intra- and interspecific variation in spectral properties of dominant Sphagnum moss species in boreal peatlands. Ecol. Evol. 13, e10197 https://doi.org/10.1002/ECE3.10197.
Schaepman-Strub, G., Limpens, J., Menken, M., Bartholomeus, H.M., Schaepman, M.E., 2009. Towards spatial assessment of carbon sequestration in peatlands: spectroscopy based estimation of fractional cover of three plant functional types. Biogeosciences 6, 275–284. https://doi.org/10.5194/BG-6-275-2009.
Šimanauskienė, R., Linkevičienė, R., Bartold, M., Dąbrowska-Zielińska, K., Slavinskienė, G., Veteikis, D., Taminskas, J., 2019. Peatland degradation: the relationship between raised bog hydrology and normalized difference vegetation index. Ecohydrology 12. https://doi.org/10.1002/ECO.2159.
Strachan, I.B., Pelletier, L., Bonneville, M.C., 2016. Inter-annual variability in water table depth controls net ecosystem carbon dioxide exchange in a boreal bog. Biogeochemistry 127, 99–111. https://doi.org/10.1007/S10533-015-0170-8/TABLES/2.
Sulman, B.N., Desai, A.R., Saliendra, N.Z., Lafleur, P.M., Flanagan, L.B., Sonnentag, O., MacKay, D.S., Barr, A.G., Van Der Kamp, G., 2010. CO2 fluxes at northern fens and bogs have opposite responses to inter-annual fluctuations in water table. Geophys. Res. Lett. 37 https://doi.org/10.1029/2010GL044018.
Sulman, B.N., Desai, A.R., Schroeder, N.M., Ricciuto, D., Barr, A., Richardson, A.D., Flanagan, L.B., Lafleur, P.M., Tian, H., Chen, G., Grant, R.F., Poulter, B., Verbeeck, H., Ciais, P., Ringeval, B., Baker, I.T., Schaefer, K., Luo, Y., Weng, E., 2012. Impact of hydrological variations on modeling of peatland CO2 fluxes: results from the North American Carbon Program site synthesis. J. Geophys. Res. Biogeosci. 117, 1031. https://doi.org/10.1029/2011JG001862.
Swindles, G.T., Morris, P.J., Mullan, D.J., Payne, R.J., Roland, T.P., Amesbury, M.J., Lamentowicz, M., Turner, T.E., Gallego-Sala, A., Sim, T., Barr, I.D., Blaauw, M., Blundell, A., Chambers, F.M., Charman, D.J., Feurdean, A., Galloway, J.M., Gałka, M., Green, S.M., Kajukało, K., Karofeld, E., Korhola, A., Lamentowicz, Ł., Langdon, P., Marcisz, K., Mauquoy, D., Mazei, Y.A., McKeown, M.M., Mitchell, E.A. D., Novenko, E., Plunkett, G., Roe, H.M., Schoning, K., Sillasoo, Ü., Tsyganov, A.N., van der Linden, M., Väliranta, M., Warner, B., 2019. Widespread drying of European peatlands in recent centuries. Nat. Geosci. 12, 922–928. https://doi.org/10.1038/s41561-019-0462-z.
Taddeo, S., Dronova, I., Depsky, N., 2019. Spectral vegetation indices of wetland greenness: responses to vegetation structure, composition, and spatial distribution. Remote Sens. Environ. 234, 111467 https://doi.org/10.1016/J.RSE.2019.111467.
Toca, L., Morrison, K., Artz, R.R.E., Gimona, A., Quaife, T., 2022. High resolution C-band SAR backscatter response to peatland water table depth and soil moisture: a laboratory experiment. Int. J. Remote Sens. 43, 5231–5251. https://doi.org/10.1080/01431161.2022.2131478.

Tucker, C., O'Neill, A., Meingast, K., Bourgeau-Chavez, L., Lilleskov, E., Kane, E.S., 2022. Spectral indices of vegetation condition and soil water content reflect controls on CH4 and CO2 exchange in Sphagnum-dominated northern peatlands. J. Geophys. Res. Biogeosci. 127 https://doi.org/10.1029/2021JG006486 e2021JG006486.

Van den Hoof, C., Lambert, F., 2016. Mitigation of drought negative effect on ecosystem productivity by vegetation mixing. J. Geophys. Res. Biogeosci. 121, 2667–2683. https://doi.org/10.1002/2016JG003625.

Van Gaalen, K.E., Flanagan, L.B., Peddle, D.R., 2007. Photosynthesis, chlorophyll fluorescence and spectral reflectance in Sphagnum moss at varying water contents. Oecologia 153, 19–28. https://doi.org/10.1007/S00442-007-0718-Y/FIGURES/5.

Vereecken, H., Amelung, W., Bauke, S.L., Bogena, H., Brüggemann, N., Montzka, C., Vanderborght, J., Bechtold, M., Blöschl, G., Carminati, A., Javaux, M., Konings, A.G., Kusche, J., Neuweiler, I., Or, D., Steele-Dunne, S., Verhoef, A., Young, M., Zhang, Y., 2022. Soil hydrology in the Earth system. Nat. Rev. Earth Environ 39 (3), 573–587. https://doi.org/10.1038/s43017-022-00324-6.

Vogelmann, J.E., Moss, D.M., 1993. Spectral reflectance measurements in the genus Sphagnum. Remote Sens. Environ. 45, 273–279. https://doi.org/10.1016/0034-4257(93)90110-J.

Walther, S., Duveiller, G., Jung, M., Guanter, L., Cescatti, A., Camps-Valls, G., 2019. Satellite observations of the contrasting response of trees and grasses to variations in water availability. Geophys. Res. Lett. 46, 1429–1440. https://doi.org/10.1029/2018GL080535.

Wang, L., Qu, J.J., Hao, X., Zhu, Q., 2008. Sensitivity studies of the moisture effects on MODIS SWIR reflectance and vegetation water indices, 29, pp. 7065–7075. https://doi.org/10.1080/01431160802226034.

White, H.J., Gaul, W., Sadykova, D., León-Sánchez, L., Caplat, P., Emmerson, M.C., Yearsley, J.M., 2019. Land cover drives large scale productivity-diversity relationships in Irish vascular plants. PeerJ 2019, e7035. https://doi.org/10.7717/PEERJ.7035/SUPP-2.

Wilson, P., 2012. The Relationship among Micro-Topographic Variation, Water Table Depth and Biogeochemistry in an Ombrotrophic Bog. McGill University, Montreal.

Wilson, D., Mackin, F., Tuovinen, J.P., Moser, G., Farrell, C., Renou-Wilson, F., 2022. Carbon and climate implications of rewetting a raised bog in Ireland. Glob. Chang. Biol. 28, 6349–6365. https://doi.org/10.1111/GCB.16359.

Yli-Halla, M., Lötjönen, T., Kekkonen, J., Virtanen, S., Marttila, H., Liimatainen, M., Saari, M., Mikkola, J., Suomela, R., Joki-Tokola, E., 2022. Thickness of peat influences the leaching of substances and greenhouse gas emissions from a cultivated organic soil. Sci. Total Environ. 806, 150499 https://doi.org/10.1016/J.SCITOTENV.2021.150499.

Yu, Z., Loisel, J., Brosseau, D.P., Beilman, D.W., Hunt, S.J., 2010. Global peatland dynamics since the Last Glacial Maximum. Geophys. Res. Lett. 37 https://doi.org/10.1029/2010GL043584.

Zhang, H., Väliranta, M., Swindles, G.T., Aquino-López, M.A., Mullan, D., Tan, N., Amesbury, M., Babeshko, K.V., Bao, K., Bobrov, A., Chernyshov, V., Davies, M.A., Diaconu, A.C., Feurdean, A., Finkelstein, S.A., Garneau, M., Guo, Z., Jones, M.C., Kay, M., Klein, E.S., Lamentowicz, M., Magnan, G., Marcisz, K., Mazei, N., Mazei, Y., Payne, R., Pelletier, N., Piilo, S.R., Pratte, S., Roland, T., Saldaev, D., Shotyk, W., Sim, T.G., Sloan, T.J., Słowiński, M., Talbot, J., Taylor, L., Tsyganov, A.N., Wetterich, S., Xing, W., Zhao, Y., 2022. Recent climate change has driven divergent hydrological shifts in high-latitude peatlands. Nat. Commun. 131 (13), 1–7. https://doi.org/10.1038/s41467-022-32711-4.

Zhong, Y., Jiang, M., Middleton, B.A., 2020. Effects of water level alteration on carbon cycling in peatlands. https://doi.org/10.1080/20964129.2020.1806113.